Formation Mechanism of the ENSO-Independent Summer Western North Pacific Anomalous Anticyclone

TONG LU,[a,b,c] ZHIWEI ZHU,[a,b] YING YANG,[a] JING MA,[a] AND GANG HUANG[b,c]

[a] *Key Laboratory of Meteorological Disaster, Ministry of Education (KLME)/ Joint International Research Laboratory of Climate and Environment Change (ILCEC)/ Collaborative Innovation Center on Forecast and Evaluation of Meteorological Disasters (CIC-FEMD), Nanjing University of Information Science and Technology, Nanjing, China*

[b] *State Key Laboratory of Numerical Modeling for Atmospheric Sciences and Geophysical Fluid Dynamics, Institute of Atmospheric Physics, Chinese Academy of Sciences, Beijing, China*

[c] *University of Chinese Academy of Sciences, Beijing, China*

(Manuscript received 14 April 2022, in final form 31 October 2022)

ABSTRACT: The western North Pacific anomalous anticyclone (WNPAC) is the key circulation modulating the East Asian summer climate. In this study, the formation mechanism of the summer WNPAC that is independent of El Niño–Southern Oscillation (ENSO) is investigated. Although ENSO has a significant relationship with WNPAC, except for the super El Niño years, the WNPAC index remains almost unchanged after removing ENSO's impact, suggesting the possibility of other origins of the WNPAC apart from ENSO. An Atlantic-to-Pacific two-step mechanism is proposed for the formation of ENSO-independent summer WNPAC. In boreal spring, diabatic heating induced by the positive sea surface temperature anomalies (SSTAs) over the tropical Atlantic could stimulate a stationary equivalent barotropic Rossby wave train that travels across the Eurasian continent and ends in the tropical North Pacific. At the end of the Rossby wave train, the lower-level anomalous anticyclone advects negative moist enthalpy into the equator, which suppresses the local convection over the tropical North Pacific and equatorial central Pacific, and thus triggers the lower-level equatorial easterly anomaly to its west. During boreal summer, the lower-level easterly anomaly leads to the zonal dipole SSTA pattern with a negative center in the tropical central Pacific and a positive one in the Maritime Continent. Then, this dipole SSTA pattern over the Pacific exerts a relaying effect that further reinforces and westward shifts the dipole convection anomaly pattern, generating the WNPAC as a Gill-type response. This study underpins the independent role of Atlantic oceanic forcing through the extratropical route in the formation of ENSO-independent summer WNPAC.

SIGNIFICANCE STATEMENT: By linearly removing ENSO's impact on summer monthly sea surface temperature anomalies (SSTAs), this study explores the sources of summer western North Pacific anomalous anticyclone (WNPAC) apart from ENSO. It is found that the high correlation between WNPAC and ENSO largely depends on the super El Niño events, and the origin of the ENSO-independent WNPAC is rooted in the tropical Atlantic oceanic forcing. The positive tropical Atlantic SSTAs in spring can independently induce atmospheric teleconnection from the North Atlantic to the North Pacific through the extratropical route, which triggers anomalous easterlies over the equatorial Pacific via suppressed local convection caused by the dry air advection over the North Pacific. The equatorial easterlies enhance the dipole anomalous SST and convection pattern over the Maritime Continent and tropical western/central Pacific in summer, which finally stimulates the WNPAC. The result emphasizes the independent role of tropical Atlantic SSTAs in the formation of summer WNPAC, thus providing a new perspective for the seasonal prediction of East Asian summer climate.

KEYWORDS: Atlantic Ocean; ENSO; Atmosphere-ocean interaction; Interannual variability

1. Introduction

As the strongest climate mode on the interannual time scale, El Niño–Southern Oscillation (ENSO) exerts significant remote impacts on East Asian climate (Huang and Wu 1989; Zhang et al. 1996, 1999; Wang and Chan 2002; Wu et al. 2003; Chou et al. 2009; Wang et al. 2017). The western North Pacific anomalous anticyclone (WNPAC; also referred to as the anomalous Philippine Sea anticyclone) (Wang et al. 2000; Chou 2004; Li et al. 2017) acts as the atmospheric bridge connecting ENSO and East Asian climate.

The WNPAC forms in fall before the peak of El Niño, and its intensity increases with the development of El Niño (Wang and Zhang 2002). Maintained from the El Niño mature phase (winter) to the El Niño decaying summer (B. Wu et al. 2009; Xie et al. 2009), it directly affects East Asian summer climate (Chang et al. 2000). For example, due to the abnormally strong WNPAC, severe floods hit the middle and lower reaches of the Yangtze River basin in the summers of 1998 and 2020 (Wang et al. 2017, 2020; Liu et al. 2020; Takaya et al. 2020; Zhang et al. 2021; Zhou et al. 2021; Tang et al. 2022),

Supplemental information related to this paper is available at the Journals Online website: https://doi.org/10.1175/JCLI-D-22-0271.s1.

Corresponding author: Zhiwei Zhu, zwz@nuist.edu.cn

DOI: 10.1175/JCLI-D-22-0271.1

and heatwaves occurred over southeast China in the summer of 2013 (Wang et al. 2014). Besides, summer WNPAC can also modulate the genesis and moving tracks of tropical cyclones over the western North Pacific (Wang et al. 2013; Wang and Wang 2019). Therefore, unraveling the dynamic origin of the interannual variability of summer WNPAC is critical to understanding the East Asian summer climate.

Previous studies have already demonstrated the mechanisms of the formation and maintenance of summer WNPAC. When warm sea surface temperature anomalies (SSTAs) appear in the equatorial central/eastern Pacific during the peak of El Niño episode, a cyclonic anomaly forms at the northwest side of the SSTA-induced diabatic heating based on the Gill-type model (Gill 1980). The anomalous northeasterly on the northwestern flank of the cyclonic anomaly strengthens the trade wind in situ. Consequently, the enhanced evaporation causes local cold SSTAs. The cold SSTAs induce local diabatic cooling, which further leads to the WNPAC to its west as a Rossby wave response (Wang et al. 2000). When the El Niño SSTAs dissipate in summer, the tropical Indian Ocean characterized by positive SSTAs and enhanced convection, which stores the effect of El Niño via zonal circulation, starts to play a critical role in driving the WNPAC via inducing a Kelvin wave response (Xie et al. 2009; B. Wu et al. 2009). Recent studies suggest that without the trade wind–SST feedback and Indian Ocean warming, the WNPAC could still be maintained according to the moisture enthalpy theory (Wu et al. 2017a,b). In addition to the influences from the tropical Pacific and Indian Ocean (Wu et al. 2010; Jiang et al. 2019), the tropical Atlantic SSTAs also impact WNPAC through the tropical Rossby wave response to the west (Ham et al. 2013; Park et al. 2022), the tropical Kevin wave response to the east (Rong et al. 2010; Jiang and Li 2021; Yu et al. 2016), and the zonally overturning circulation anomaly (Hong et al. 2014; Zuo et al. 2019). Apart from the tropical SSTA forcings, the atmospheric signals from mid-to-high latitudes, such as the Arctic Oscillation (AO; Gong et al. 2011; Gao et al. 2016) and the North Atlantic Oscillation (NAO; Z. Wu et al. 2009; Wu et al. 2012) together with its downstream effects in the form of stationary Rossby wavetrains (Enomoto 2004; Kosaka et al. 2012), can significantly influence the WNPAC. In addition, the atmospheric internal variability can also influence the WNPAC (Wang et al. 2018, 2020).

However, although several factors can lead to WNPAC formation and maintenance via different routes, it is still possible that these factors are either directly or indirectly related to ENSO. In addition, the mechanisms of Atlantic influence on WNPAC above mostly emphasize the tropical routes, the extratropical influence routes remain largely unexplored.

An unprecedented abnormal WNPAC causing severe floods over the Yangtze River basin occurred in the summer of 2020 without appearance of strong El Niño event in the preceding winter (Takaya et al. 2020; Chen et al. 2021; Qiao et al. 2021; Pan et al. 2021; Zhang et al. 2021; Zheng and Wang 2021; Zhao et al. 2022), suggesting that the WNPAC may have other origins apart from ENSO. Motivated by this conundrum, this study investigates what contributes to the interannual variability of the summer WNPAC that is independent of ENSO's impact. Here we intend to address the following questions: 1) Is there any other origin of the summer WNPAC apart from ENSO? 2) If yes, what is the physical mechanism for the formation of the ENSO-independent WNPAC?

The remaining paper is organized as follows. Section 2 introduces the data, method, and model we employed. In section 3, we present the leading mode of interannual variability of the WNPAC, and compare the associated SSTA patterns with respect to ENSO and WNPAC. Section 4 introduces the method extracting the interannual variability of summer WNPAC that is independent of ENSO. In section 5, the physical mechanism for the formation of ENSO-independent summer WNPAC is revealed. The conclusions and discussion are provided in section 6.

2. Data, method, and model

a. Data

The datasets employed in this study include 1) the global monthly sea surface temperature (SST) with a 2.0° × 2.0° horizontal resolution from the National Oceanic and Atmospheric Administration (NOAA) Extended Reconstructed SST version 5 (Huang et al. 2017); 2) the interpolated monthly outgoing longwave radiation (OLR) with a 2.5° × 2.5° horizontal resolution from NOAA (Liebmann and Smith 1996); 3) the monthly precipitation gridded at 2.5° × 2.5° horizontal resolution from the Global Precipitation Climatology Project (Adler et al. 2003); 4) the monthly wind and geopotential height at multiple levels with a horizontal resolution of 2.5° × 2.5° from the National Centers for Environmental Prediction–National Center for Atmospheric Research Reanalysis (Kalnay et al. 1996); 5) the monthly wind, geopotential height, and specific humidity at multiple levels from the fifth-generation ECMWF reanalysis for the global climate and weather (ERA5; Hersbach et al. 2019) with a 2.5° × 2.5° horizontal resolution. To reduce the uncertainty from different data sources, the arithmetic means for the monthly wind and geopotential height of two datasets (NCEP–NCAR and ERA5) have been applied in this study. All datasets cover the period of 1979–2020.

b. Method

To focus on the interannual time scale, the 9-yr running means of all variables were removed first. The leading mode of East Asian summer circulation was obtained through the multivariate empirical orthogonal function (MV-EOF) analysis (Wang 1992) on the 850-hPa wind field over the East Asia–western North Pacific sector (0°–50°N, 100°–150°E). The North's test was employed to analyze the significance of the MV-EOF mode (North et al. 1982). The Student's t test was used to test the significance of the correlation coefficients and regression coefficients.

The Niño-3.4 index was calculated as the SSTA averaged over 5°S–5°N, 120°–170°W in winter (DJF). Following Wang et al. (2008), the WNPAC index (I_{WNPAC}) was defined as the 850-hPa zonal wind contrast between 22.5°–32.5°N, 110°–140°E and 5°–15°N, 90°–130°E.

A linear regression analysis method was used to exclude the influence of ENSO (Gong et al. 2011; Gao et al. 2014): $X_{\mathrm{NoEN}} = X - I_{\mathrm{EN}} \times \mathrm{Reg}(X \text{ onto } I_{\mathrm{EN}})$. Here, I_{EN} denotes the indices representing the impact from ENSO, and X represents the original variables. Therefore, $I_{\mathrm{EN}} \times \mathrm{Reg}(X \text{ onto } I_{\mathrm{EN}})$ denotes the reconstruction fields with ENSO's impact, and the X_{NoEN} indicates the variable fields that are independent of I_{EN}.

To explore the atmospheric teleconnections associated with the ENSO-independent WNPAC, the Rossby wave activity flux (WAF) was calculated based on the following formula (Takaya and Nakamura 2001):

$$\mathbf{W} = \frac{1}{2|\overline{\mathbf{U}}|}\begin{bmatrix} \overline{u}(\psi_x'^2 - \psi'\psi_{xx}') + \overline{v}(\psi_x'\psi_y' - \psi'\psi_{xy}') \\ \overline{u}(\psi_x'\psi_y' - \psi'\psi_{xy}') + \overline{v}(\psi_y'^2 - \psi'\psi_{yy}') \end{bmatrix}. \quad (1)$$

Among them, ψ and $\mathbf{U} = (u, v)$ represent the streamfunction and the horizontal wind, respectively, and $\mathbf{W}$ refers to the two-dimensional Rossby WAF. The overbar and the prime represent the climatological mean and the anomaly, respectively.

Vertical motions are constrained by moist static energy (MSE) budget balance in the tropics (Neelin and Held 1987). To investigate the moist enthalpy advection process for the formation of ENSO-independent WNAPC, the horizontal advection of climatological moist enthalpy by anomalous wind $\langle -\mathbf{u}' \cdot \nabla_h \overline{(c_p T + L_v q)} \rangle$ from the simplified MSE equation (Neelin 2007; Wu et al. 2017a) was calculated. The simplified MSE equation was written as

$$\langle \omega' \partial_p \overline{h} \rangle \approx F_{\mathrm{net}}' - \langle \overline{\mathbf{u}} \cdot \nabla_h (c_p T + L_v q)' \rangle - \langle \mathbf{u}' \cdot \nabla_h \overline{(c_p T + L_v q)} \rangle - \langle \overline{\omega} \partial_p h' \rangle + \mathrm{NL}. \quad (2)$$

Here, angle brackets represent the mass integral from 1000 to 100 hPa; $\mathbf{u}$ and ω denote horizontal wind and vertical pressure velocity, respectively; $h = c_p T + L_v q + \varphi$ represents MSE; $c_p T + L_v q$ indicates the moist enthalpy; T, q and φ denote air temperature, specific humidity, and geopotential, respectively; c_p and L_v denote the specific heat at constant pressure (1004 J K^{-1} kg^{-1}) and the latent heat of vaporization (taken constant at 2.5×10^6 J kg^{-1}). Therefore, the anomalous vertical advection of climatological MSE is denoted by $\langle \omega' \partial_p \overline{h} \rangle$, F_{net} represents the net MSE flux coming into the atmospheric column from 1000 to 100 hPa, $-\langle \overline{\mathbf{u}} \cdot \nabla_h (c_p T + L_v q)' \rangle$ denotes the climatological horizontal advection of anomalous moist enthalpy, $\langle -\mathbf{u}' \cdot \nabla_h \overline{(c_p T + L_v q)} \rangle$ represents the anomalous horizontal advection of climatological moist enthalpy, $-\langle \overline{\omega} \partial_p h' \rangle$ denotes the climatological vertical advection of anomalous MSE, and NL represents the sum of all the nonlinearly terms.

According to Wu et al. (2017a), moisture advection, rather than temperature advection, primarily contributes to the $\langle -\mathbf{u}' \cdot \nabla_h \overline{(c_p T + L_v q)} \rangle$ term in the tropical western North Pacific (WNP; >84%). Therefore, $\langle -\mathbf{u}' \cdot \nabla_h \overline{(L_v q)} \rangle$ was employed to represent $\langle -\mathbf{u}' \cdot \nabla_h \overline{(c_p T + L_v q)} \rangle$ to examine the main process of moist enthalpy advection.

c. Model

To further unravel the physical mechanism for the formation of ENSO-independent WNPAC, two general circulation models were utilized in this study. One is the anomaly atmospheric general circulation model (AGCM; Held and Suarez 1994), which was developed from the global spectrum dry AGCM of the Geophysical Fluid Dynamics Laboratory. This five-layer intermediate complex model uses sigma ($\sigma = p/p_s$) as its vertical coordinate and has a T42 Gaussian grid horizontal resolution. The basic equations include the momentum, continuity, thermal dynamic, and hydrostatic equations. To mimic the observed heating profile, different heating rates were prescribed at different levels of the troposphere in the model. The long-term climatological mean derived from the NCEP–NCAR reanalysis is employed to be the model background state. This AGCM has been widely used to validate the formation of various atmospheric teleconnection patterns (Zhu and Li 2016, 2018; Lu et al. 2020). The other one is the linear baroclinic model (LBM), which is based on the primary equation model developed by Watanabe and Kimoto (2000). This model is run at a resolution of triangular truncation of T42 with 20 sigma levels in the vertical. The model has also been widely employed to investigate atmospheric circulation response to the anomalous heating (Sampe and Xie 2010; Zhang et al. 2016; Wang et al. 2022). Both of the two models were integrated for 60 days, and the averaged output in the last 10 days was considered as the equilibrium state.

3. Interannual variability of the summer WNPAC

a. The leading mode of WNPAC interannual variability

Figure 1a shows the spatial pattern of the first EOF mode for the interannual component of 850-hPa zonal and meridional wind field over the East Asia and WNP sector in summer. This leading mode accounts for 51% of the total variance, which is statistically significant and independent from other modes (North et al. 1982). The spatial pattern of this mode features a robust western North Pacific anomalous anticyclone (WNPAC). Negative precipitation anomalies can be observed under the main body of the WNPAC, whereas positive precipitation anomalies appear over the southern and northern flanks of the WNPAC. Particularly, prominent southwesterly on the northwest flank of the WNPAC advects the warm and moist air from the tropical ocean to the middle and lower reaches of the Yangtze River basin, the Korean Peninsula, and southern Japan, resulting in the mei-yu/changma/baiu during the peak stage of East Asian summer monsoon.

Figure 1b shows that the principal component of this mode (PC1) is highly coherent with the WNPAC index (I_{WNPAC}) with a correlation coefficient of 0.95 ($P < 0.01$), verifying that the I_{WNPAC} index can nicely represent the WNPAC interannual variability. Therefore, in the following article, the I_{WNPAC} index is employed to represent the interannual variation of WNPAC. It is noteworthy that PC1 has a close relationship with the preceding winter mean Niño-3.4 index ($R = 0.43$, $P < 0.01$), suggesting the significant linkage between WNPAC and ENSO (Chou 2004; Li et al. 2017). However, it should be noted that some years are quite deviated from the fitting line, indicating the likelihood of an unreliable ENSO–WNPAC relationship.

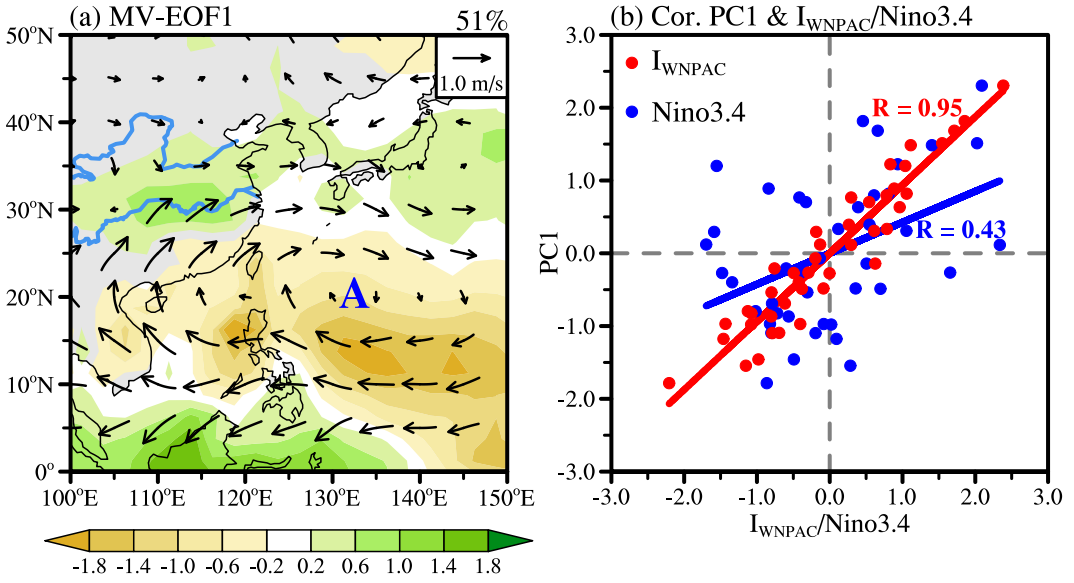

FIG. 1. (a) Spatial pattern of the first MV-EOF mode of the 850-hPa winds over the domain 0°–50°N, 100°–150°E for the period of 1979–2020. (b) The scatterplot for the principal component (PC) with respect to the I_{WNPAC} (red dots) and Niño-3.4 (blue dots) index. Shadings in (a) are the summer mean precipitation (mm day^{-1}) regressed onto PC. Letter A denotes the center of the WNPAC.

b. *Comparison of SSTAs related to ENSO and WNPAC*

Although ENSO decays in summer, its influence on WNPAC can be maintained from winter to summer through the Indian Ocean capacitor effect. Considering that the impact of ENSO during summer may vary from month to month (Wu et al. 2010; Wang et al. 2017), we first compared the regression SSTA fields in June, July, and August onto the I_{WNPAC} indices and Niño-3.4 index, respectively (Fig. 2).

During summer, significant positive SSTAs related to ENSO are observed from the tropical Indian Ocean to the western Pacific, as well as in the tropical North Atlantic Ocean (Figs. 2a–c). Meanwhile, a basin-scale horseshoe-like SSTA pattern (similar to the interdecadal Pacific oscillation pattern) could be found over the North Pacific Ocean, and significant positive SSTAs appear in the cold tongue region. Over the equatorial central Pacific, positive SSTAs can be found in June, but they get weakened in July and dissipated in August.

In contrast, significant positive SSTAs associated with WNPAC are mainly confined in the northern Indian Ocean, western North Pacific, and tropical North Atlantic in summer (Figs. 2d–f). The weak negative SSTAs appear over the equatorial central Pacific in July and August. In addition, significant negative SSTAs are observed over the Barents Sea and Kara Sea in August (Fig. 2f).

Comparing the regressed SST patterns with respect to ENSO and WNPAC indices, only the SSTs over the tropical Indian Ocean and the western Pacific present similar features with positive anomalies, verifying that ENSO's impact on summer WNPAC is through the Indian Ocean warming. Significant differences of regressed SST patterns are over the tropical central/eastern Pacific and tropical Atlantic, indicating the possibility of other origins of WNPAC apart from ENSO. In the following section, we exclude the influence of ENSO through linearly removing the DJF Niño-3.4-related SSTAs during the following summer, to explore the formation mechanism of the ENSO-independent summer WNPAC.

4. Extraction of the WNPAC independent of ENSO

a. *Definition of ENSO's impact in the following summer*

To investigate the origin of the ENSO-independent summer WNPAC, the influence of ENSO should be removed first. As shown in Figs. 2a–c, ENSO can significantly impact the global SSTAs during the following summer. Since Niño-3.4-related SSTAs differ from June to August (Wu et al. 2010), the index of ENSO's impact (I_{EN}) was defined month by month. To comprehensively remove ENSO's impact in the following summer, I_{EN} indices are defined by the tropical averaged SSTAs weighted by regression coefficients with respect to the Niño-3.4 index passing the 95% confidence level. Note that because the I_{EN} indices are spatially weighted, they can also reflect the tropical SSTA pattern (such as IOBM and other SST modes) related to ENSO.

Based on the regressed SST onto the Niño-3.4 index over the tropical region (30°S–30°N in Figs. 2a–c), the monthly I_{EN} indices were calculated as follows:

$$I_{EN} = \frac{SST_1 b_1 + SST_2 b_2 + \cdots + SST_n b_n}{b_1 + b_2 + \cdots + b_n}. \quad (3)$$

Here, n represents the number of significant grids, b_k ($k = 1, 2, \ldots, n$) refers to the kth regression coefficient (passing the 95% confidence level), and SST_k denotes the corresponding SSTA.

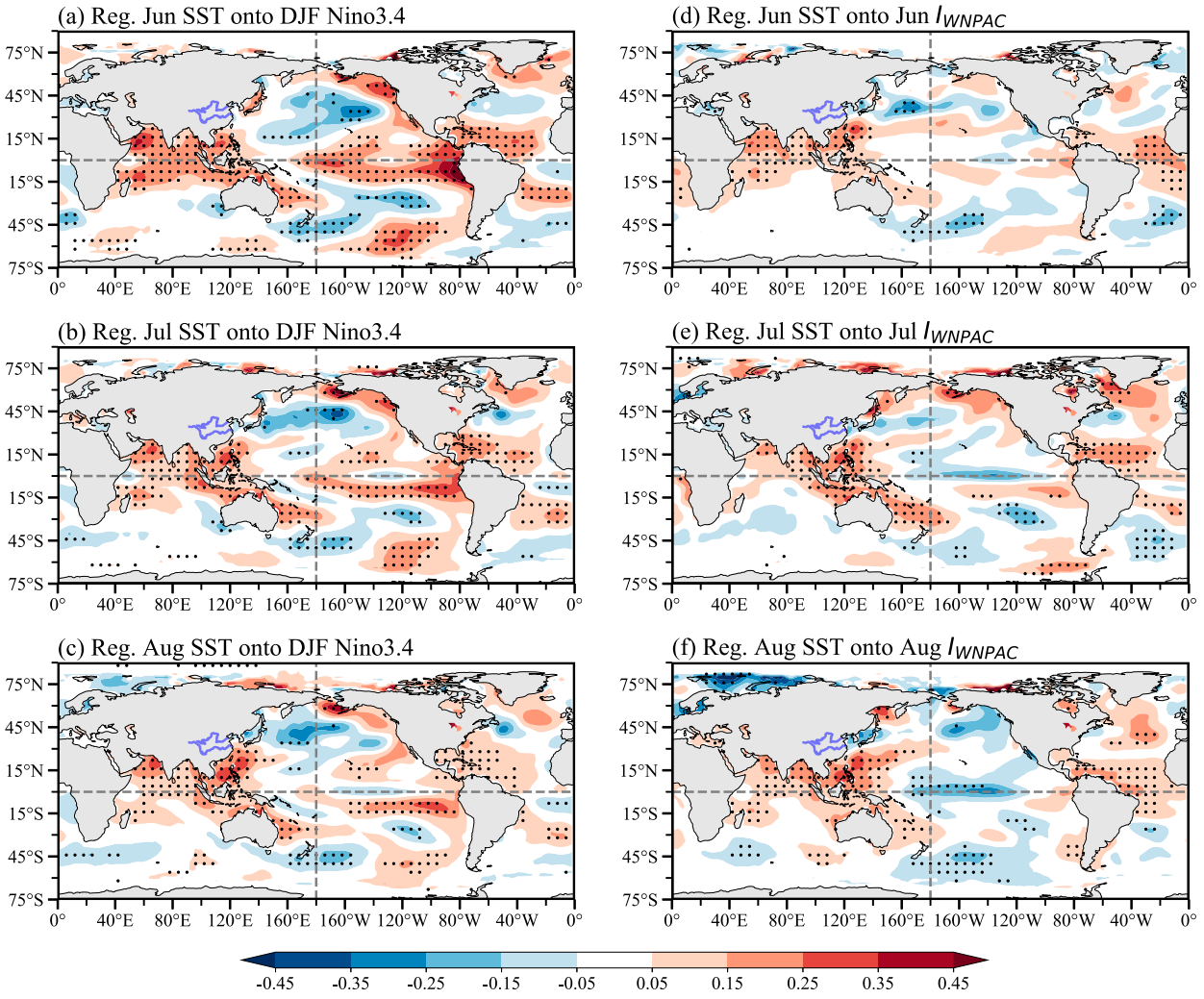

FIG. 2. The global SST (shading; °C) in (a) June, (b) July, and (c) August regressed onto the DJF Niño-3.4 index. (d)–(f) As in (a)–(c), respectively, but onto the WNPAC index. Stippled areas indicate regression coefficients passing the 95% confidence level. The vertical and horizontal dashed lines denote the 180° meridian and the equator, respectively.

It is noteworthy that since SSTAs over the extratropics usually result from the passive response to the tropical forcing, the influence of the ENSO-related tropical SSTAs would be weakened with the inclusion of SSTAs outside the tropics. Therefore, the I_{EN} indices are derived only from 30°S to 30°N.

To further confirm whether the I_{EN} indices could well represent ENSO's impacts in each month of summer, the correlation coefficients between summer monthly I_{EN} indices and the DJF Niño-3.4 index were calculated. As shown in Table 1, all the I_{EN} indices within summer are highly correlated with the DJF Niño-3.4 index. Interestingly, although the correlation coefficient between summer mean I_{WNPAC} index and Niño-3.4 index is 0.52 ($P < 0.05$), no significant relationship can be found between August I_{WNPAC} and Niño-3.4. The correlation coefficient between Niño-3.4 and I_{WNPAC} index in June (0.35) is also lower than that between Niño-3.4 index and the summer mean I_{WNPAC} index (0.52). Only the I_{WNPAC} index in July shows a robust relationship to the Niño-3.4 index ($R = 0.63$, $P < 0.01$). In contrast, I_{WNPAC} is significantly correlated with I_{EN} in August ($R = 0.51$, $P < 0.01$), indicating that ENSO has an indirect influence on the maintenance of the WNPAC in August. In June and July, the correlation

TABLE 1. Correlation coefficients among the indices (boldface values indicate those passing the 95% confidence level).

	Niño-3.4	I_{EN}_6	I_{EN}_7	I_{EN}_8
Niño-3.4	**1**	**0.81**	**0.84**	**0.77**
I_{WNPAC}_6	**0.35**	**0.32**		
I_{WNPAC}_7	**0.63**		**0.62**	
I_{WNPAC}_8	0.23			**0.51**
$I_{WNPAC\_NoEN}\_6$	0.10	0.00		
$I_{WNPAC\_NoEN}\_7$	0.14		0.00	
$I_{WNPAC\_NoEN}\_8$	−0.18			0.00

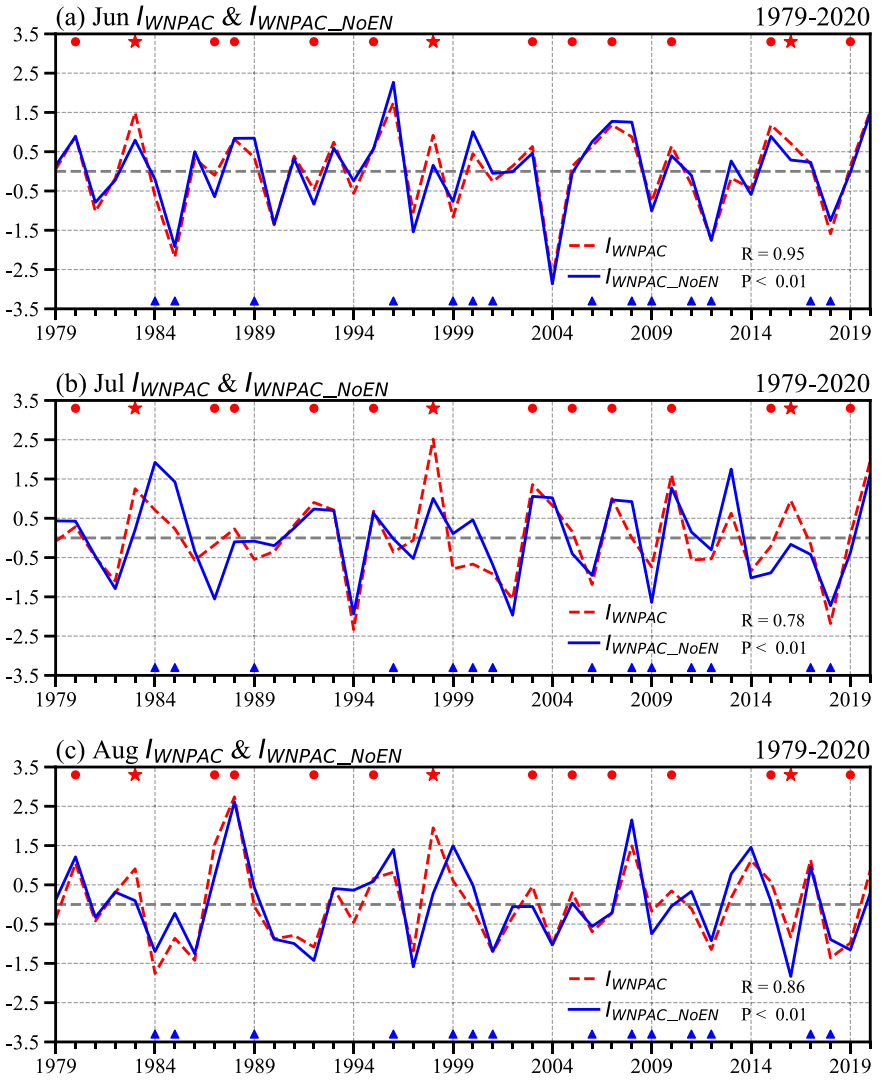

FIG. 3. The standardized WNPAC index (I_{WNPAC}; red dashed lines) and the WNPAC index after removing ENSO's impact (I_{WNPAC_NoEN}; blue solid lines) in (a) June, (b) July, and (c) August. The red dots and blue triangles denote the El Niño and La Niña years, respectively. The red stars represent the three super El Niño years of 1983, 1998, and 2016.

coefficient between I_{WNPAC} and I_{EN} has no distinct difference from that between I_{WNPAC} index and the Niño-3.4 index, whereas in August the former is much higher compared to the latter, suggesting that the monthly I_{EN} indices could better represent the direct and indirect impacts of the preceding ENSO comparing with Niño-3.4 index.

b. *Interannual variability of the ENSO-independent WNPAC*

The analyses above indicate that the I_{EN} indices in the summer months could nicely represent ENSO's impact during ENSO decaying summer. After removing the impact of ENSO through $X_{NoEN} = X - I_{EN} \times \text{Reg}(X \text{ onto } I_{EN})$, the monthly I_{WNPAC} indices independent of ENSO (I_{WNPAC_NoEN}) are obtained. Table 1 shows that the monthly I_{WNPAC_NoEN} indices are correlated with neither Niño-3.4 index nor the corresponding I_{EN} indices, suggesting that the I_{WNPAC_NoEN} indices are entirely independent of ENSO.

What are the differences in I_{WNPAC} index before and after removing the impact of ENSO? Fig. 3 shows the year-to-year variability of the monthly I_{WNPAC} (red dashed lines) and I_{WNPAC_NoEN} (blue solid lines) indices. It is clear that the I_{WNPAC} and I_{WNPAC_NoEN} indices share much in common with only slight differences appearing in specific super El Niño years (i.e., 1983, 1998 and 2016). The high correlation coefficients between I_{WNPAC} and I_{WNPAC_NoEN} indices imply that ENSO can only explain limited variability of WNPAC, and the WNPAC may have other origins apart from ENSO. We further defined the thresholds to measure the differences between monthly I_{WNPAC} and I_{WNPAC_NoEN} indices (Table S1 in the

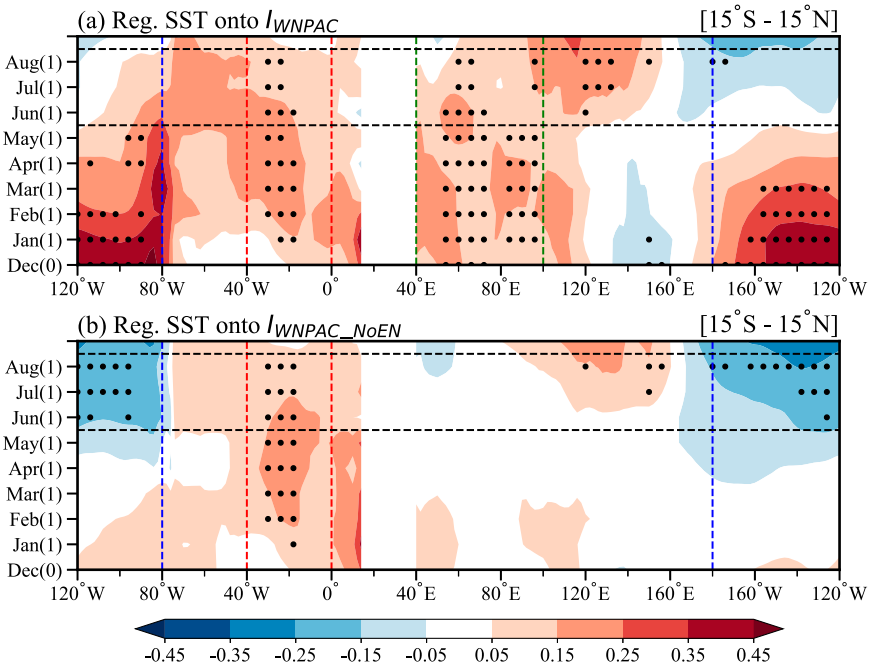

FIG. 4. Regressed monthly SSTA (°C) averaged over 15°S–15°N from December(0) to August(1) onto the summer mean (a) I_{WNPAC} and (b) I_{WNPAC_NoEN}. The black dashed box indicates June–August. The red, blue, and green dashed boxes represent the tropical Atlantic, central/eastern Pacific, and Indian Oceans. Stippled areas indicate values passing the 90% confidence level.

online supplemental material). The differences between I_{WNPAC} and I_{WNPAC_NoEN} indices are larger in super El Niño years (marked as red stars; 1983, 1998, and 2016) than those in normal El Niño years (marked as red dots) and La Niña years (marked as blue triangles), indicating again that only super El Niño events can strongly affect the summer WNPAC (Wang et al. 2017).

Note that the correlation coefficients between WNPAC and I_{EN} indices drop to zero after the exclusion of ENSO (Table 1) under the context of the almost unchanged I_{WNPAC} indices. This is because the changes of the dots representing the correlation between I_{EN} indices and I_{WNPAC}/I_{WNPAC_NoEN} indices in super El Niño years (such as 1983 and 1998) can lead to the drops in the relations of WNPAC indices and ENSO (Fig. S1). The correlation coefficients between the I_{WNPAC} and I_{WNPAC_NoEN} indices and their intensity retain the same feature as those without being standardized (Fig. S2), suggesting the robustness of the result.

The reason for removing the influence of ENSO on the WNPAC month by month is that ENSO has different impacts on WNPAC within summer (Wu et al. 2010). For example, positive values of I_{WNPAC} indices occur in June and July of 2016, but a negative one appears in August. Large values of I_{WNPAC} can be found in July and August of 1998, whereas June shows a much smaller value. Meanwhile, similar values of I_{WNPAC} indices can be observed in each month of 1983, but a larger difference can be found between the I_{WNPAC} index and I_{WNPAC_NoEN} index in July. During 2016, after removing ENSO's impact, the value of the resultant I_{WNPAC_NoEN} index retains positive for June, but turns negative in July. Note that we also directly exclude the summer mean influence of ENSO (Fig. S3) and compare the indices before and after removing ENSO (Fig. S4). The results are consistent to those based on removing ENSO's impact month by month.

Unlike the large differences between the I_{WNPAC} and I_{WNPAC_NoEN} indices in 1983, 1998, and 2016, the high values of the I_{WNPAC} indices in each month of 2020 are almost unchanged after removing ENSO's impact, corresponding to the absence of super El Niño for the strong summer WNPAC in 2020. This indeed indicates that the strong I_{WNPAC} indices in 2020 were not influenced by ENSO, which again inspires us to explore the origins for the formation of ENSO-independent summer WNPAC.

5. Mechanism for the formation of ENSO-independent summer WNPAC

As shown in the above analyses, except for the super El Niño years, the interannual variability of WNPAC remains nearly unchanged after excluding the impact of ENSO. Then, what is the origin behind the interannual variability of summer mean WNPAC?

To detect the possible tropical SSTA forcings of WNPAC, the time evolution of tropical mean (15°S–15°N) SSTAs with respect to the summer mean I_{WNPAC} and I_{WNPAC_NoEN} indices from the preceding December to August is plotted (Fig. 4). The I_{WNPAC} index is related to the positive SSTAs in the tropical central and eastern Pacific, which peak in the previous winter

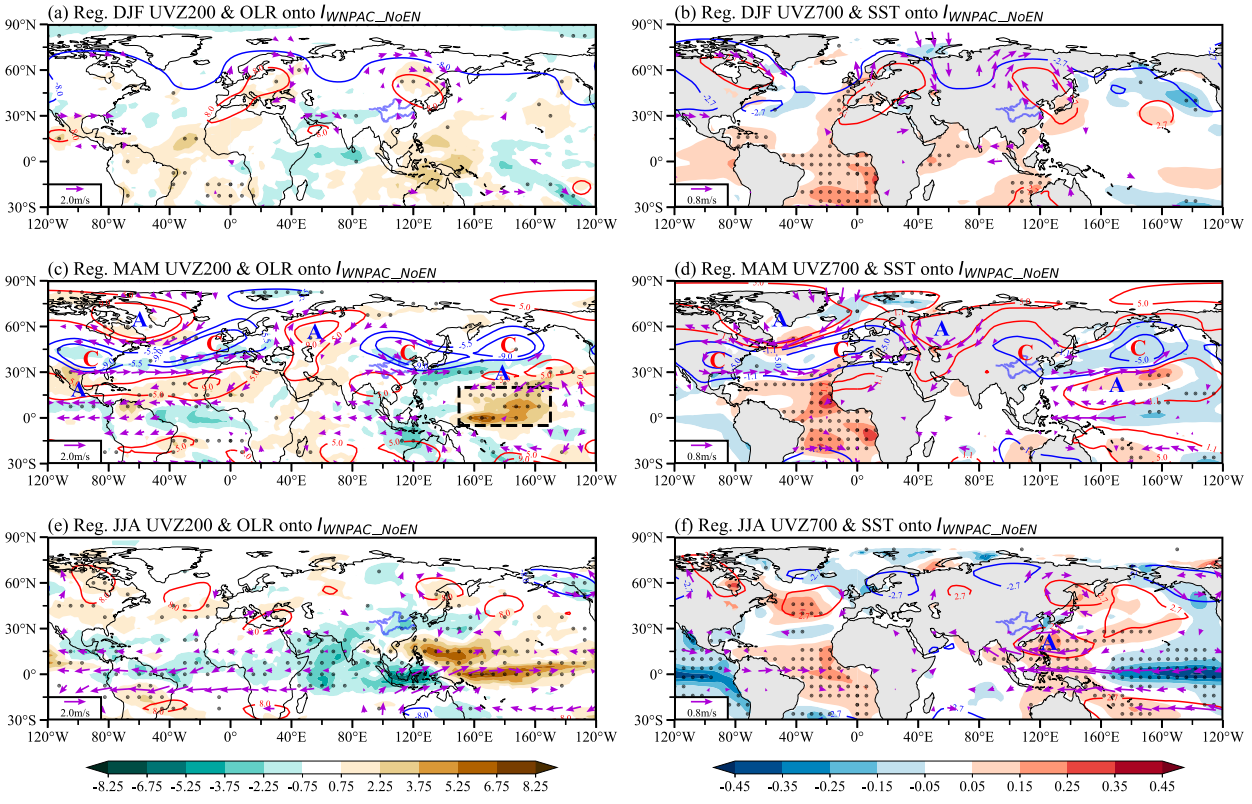

FIG. 5. Regressed (a) 200-hPa wind (vectors; m s^{-1}), geopotential height (contours; gpm), and OLR (shading; W m^{-2}), and (b) 700-hPa wind (vectors; m s^{-1}), geopotential height (contours; gpm), and SST (shading; °C) in DJF onto I_{WNPAC_NoEN}. (c),(d) and (e),(f) As in (a) and (b) but for spring (MAM) and summer (JJA), respectively. The letters A and C denote the center of the anticyclonic and cyclonic anomalies, respectively. Stippled areas and vectors indicate values passing the 90% confidence level. The black dashed box (5°S–20°N, 150°E–150°W) in (c) denotes the tropical central North Pacific and equatorial Pacific area with significant positive OLR anomalies.

and dissipate in spring. The positive SSTAs over the tropical Indian Ocean persist from winter to the following summer (Fig. 4a), indicating that the Indian Ocean capacitor effect can sustain ENSO's impact on the WNPAC (Xie et al. 2009; Yang et al. 2010). Besides, positive SSTAs associated with I_{WNPAC} also appear over the Atlantic from late winter and persist to summer.

In contrast, after excluding ENSO's impact (Fig. 4b), no significant SSTA signals associated with WNPAC can be found over the tropical Pacific during winter and summer, and over the tropical Indian Ocean from winter to summer, which confirms that ENSO's impact has been completely removed. However, it is worth noting that significant positive SSTAs persisting from January to August can still be found over the Atlantic. Following the Atlantic warming in spring, negative SSTAs start to develop over the Pacific during the spring season, suggesting that the Atlantic SSTA forcing could exert a remote impact on Pacific (Rong et al. 2010; Lu et al. 2020; Exarchou et al. 2021; Jiang and Li 2021; Chen et al. 2022; Yang et al. 2023). Therefore, we speculate that the driver of the ENSO-independent WNPAC interannual variation may be the tropical Atlantic oceanic forcing. In the following article, the physical mechanism of the Atlantic SSTA oceanic forcing on the formation of ENSO-independent WNPAC is explored.

Figure 5 shows the atmospheric circulation, SST, and OLR anomalies associated with the ENSO-independent WNPAC from the previous winter to summer. Consistent with Fig. 4, the most significant SSTAs exist over tropical southern Atlantic Ocean during winter, whereas no significant SSTA can be found in the tropical Pacific Ocean (Figs. 5a,b). Likewise, in spring (Figs. 5c,d) no significant SSTA can be found in the tropical Pacific Ocean and Indian Ocean because of the removal of ENSO's impact. However, it can be clearly seen that the positive SSTAs over the Atlantic are further intensified and extended to cover the entire tropical Atlantic Ocean. Note that the remarkable positive Atlantic SSTAs are accompanied by an equivalent barotropic Rossby wave train dominating the mid-to-high latitudes of Northern Hemisphere. This Rossby wave train is characterized by six anomalous cyclones or anticyclones, which are centered respectively over North America, southern Greenland, western Europe, the western Siberian Plain, Northeast Asia, and the tropical North Pacific. On the southeastern flank of the barotropic anticyclone over the tropical North Pacific, lower-level anomalous northeasterly appears with the remarkably suppressed convection over the tropical central North Pacific and equatorial central Pacific (Figs. 5c,d).

In summer (Figs. 5e,f), although the positive Atlantic SSTAs have become weakened (also see Fig. 4b), they remain

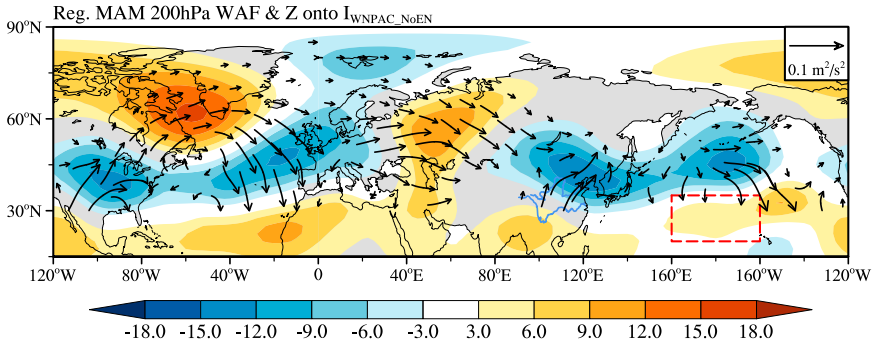

FIG. 6. Regressed MAM 200-hPa wave activity flux (vectors; $m^2\ s^{-2}$) and geopotential height (shading; gpm) onto the JJA I_{WNPAC_NoEN} index. The red dashed box (20°–35°N, 160°E–160°W) represents the location of the anomalous anticyclone over 700 hPa in the tropical North Pacific.

significant and are confined to a narrower tropical Atlantic region. The Rossby wave train dissipates without significant atmospheric circulation signals over the mid-to-high latitudes in Northern Hemisphere. Instead, the tropical Pacific presents a remarkable zonal dipole SSTA pattern with positive (negative) anomalies in the Maritime Continent (the tropical central and eastern Pacific). Accompanied by this zonal dipole SSTA pattern, strong anomalous easterly wind dominates the equator from 120°W to 120°E, leading to convergence/enhanced convection (negative OLR anomalies) over the Maritime Continent and divergence/suppressed convection (positive OLR anomalies) over the equatorial western and central Pacific. Therefore, the lower-level anticyclone anomaly over the western North Pacific (WNPAC) is formed (Fig. 5f) as a Gill-type response to the negative (positive) diabatic heating over the tropical western Pacific (Maritime Continent). Besides the Pacific SSTA dipole pattern itself, the positive Atlantic SSTAs could also induce lower-level northwesterlies over the eastern Pacific, cooling the SST via cold advection (Fig. 5f). The cold eastern Pacific could further strengthen the anomalous easterly wind over the western and central tropical Pacific, and enhance the zonal dipole anomalous SST/convection pattern via the Bjerknes feedback, thus reinforcing and maintaining the WNPAC.

It is worth mentioning that the anomalous anticyclones over the tropical Pacific during spring and summer are totally different. First, the anomalous anticyclone in spring is mainly located over the tropical North Pacific, which could hardly influence the East Asian coast. The WNPAC appears much westward, which directly influences East Asia with enhanced rainfall over the Yangtze River basin. Second, the formation of the anomalous anticyclone in spring is related to the equivalent barotropic Rossby wave train associated with positive tropical Atlantic SSTAs, whereas the WNPAC in summer is induced by the tropical diabatic heating related to the zonal dipole SSTA pattern over the Pacific.

Then, two questions arise: 1) How do the Atlantic SSTAs remotely induce the anomalous anticyclone over the tropical North Pacific during spring? 2) How does this anomalous anticyclone over the tropical North Pacific in spring transform to the WNPAC in summer?

To settle the first question, considering that the positive Atlantic SSTAs appear simultaneously with the equivalent barotropic Rossby wave train (Fig. 5c), we could speculate that the Atlantic SSTAs may influence the anomalous anticyclone over the tropical North Pacific via inducing an atmospheric teleconnection from the Atlantic to the Pacific. To support this speculation, the Rossby wave activity flux (WAF) has been calculated as shown in Fig. 6. It can be clearly seen that the WAF, which originates from North America, goes northeastward to southern Greenland, and then bends southeastward to western Europe, where it further propagates eastward, and eventually ends in the positive geopotential height (anticyclonic) anomaly over the tropical North Pacific. The positive SSTAs over the tropical Atlantic could induce convection that appears from the equatorial eastern Pacific to the Atlantic (Fig. 5c). Then, an upper-level anomalous anticyclone is stimulated over the west of the Gulf of Mexico as a Gill-type response to positive diabatic heating. The upper-level anomalous anticyclone acts as the Rossby wave source, leading to the equivalent barotropic Rossby wave train emanating from North America to the tropical North Pacific.

To further demonstrate the Atlantic oceanic forcing on the tropical North Pacific anomalous anticyclone via the Rossby wave train over the Northern Hemisphere, a numerical experiment was conducted by the AGCM. Figure 7 shows the steady state of the 200-hPa (700-hPa) geopotential height and wind response to the prescribed atmospheric heating, which is consistent with the observed positive convection over the equatorial eastern Pacific to the Atlantic. The maximum heating was set to 1 K day^{-1} at 500 hPa and reduced to the upper and lower troposphere, to mimic the vertical heating profile in observation.

Because of the diabatic heating, convergence (divergence) anomalies can be found around Central America. A Gill-type response to the diabatic heating, shown as an anticyclonic anomaly over the west of the Gulf of Mexico, is well reproduced. The anticyclonic anomaly acts as the Rossby wave source and leads to the equivalent barotropic Rossby wave train downstream from North America to the tropical North Pacific, forming the great circle route (Hoskins and Karoly 1981). The simulated Rossby wave train is similar to the

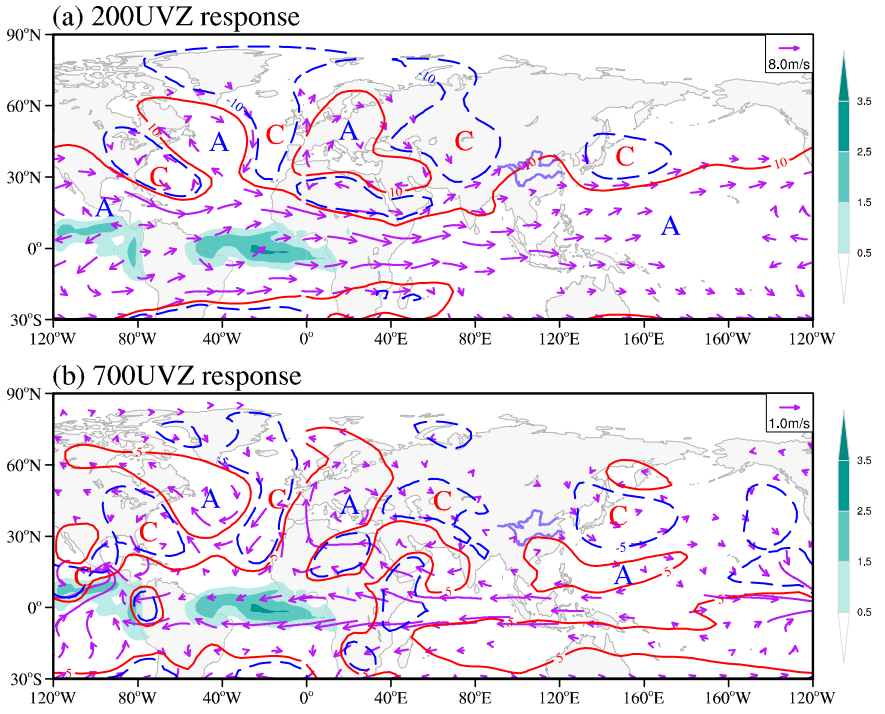

FIG. 7. The (a) 200- and (b) 700-hPa wind (vectors; m s^{-1}) and geopotential height (contours; gpm) response to the atmospheric diabatic heating over the tropical eastern Pacific to the Atlantic. The letters A and C denote the centers of the anticyclonic and cyclonic anomalies, respectively.

observation despite the slightly deviated centers of the anticyclonic and cyclonic anomalies, and this wave train follows the propagation pathway of WAF in observation (Fig. 6). Most importantly, the lower-level anomalous anticyclone over the tropical North Pacific can be well reproduced in the AGCM, verifying the independent influence of tropical Atlantic SSTAs on the atmospheric teleconnection toward the tropical North Pacific.

The strong lower-level easterlies from 40°W to 120°E over the Atlantic and Indian Ocean are induced by the diabatic heating over tropical Atlantic, which enhances the anomalous anticyclone over the tropical North Pacific through Kelvin wave response (Rong et al. 2010; Jiang and Li 2021; Yu et al. 2016). However, note that the lower-level easterlies cannot be found in the observation (Fig. 5d). Because another positive diabatic heating exists over Maritime Continent in the observation (Fig. 5c), the anomalous westerlies to the west of this heating can offset the Kelvin wave response. Therefore, the absence of the anomalous lower-level easterlies over the Atlantic and Indian Ocean in the observation does not conflict with the results of the numerical experiment.

To further verify the induced atmospheric teleconnection is not relied on model, we repeated this experiment via LBM (Watanabe and Kimoto 2000). With a specified idealized adiabatic heating centered at 4°S, 30°W, a similar equivalent barotropic Rossby wave train from North America to Pacific, as well as the anomalous tropical North Pacific anticyclone, can be reproduced (Fig. S5). The consistent results of two different models suggest that the atmospheric teleconnection induced by the Atlantic heating is not model-dependent.

After confirming that the Atlantic SSTA could induce the Rossby wave train and impact the anticyclone over the tropical Pacific, how could this lower-level anomalous anticyclone over the tropical North Pacific in spring transform to the WNPAC in summer? To answer this question, the 700-hPa climatological specific humidity and anomalous wind in spring have been regressed onto the summer mean $I_{\mathrm{WNPAC\_NoEN}}$ index.

As shown in Fig. 8, the spatial pattern of climatological specific humidity presents abundant moisture over the Indian Ocean and western Pacific warm pool region, and a strong meridional gradient around the central tropical North Pacific. The lower-level anomalous northeasterly on the southeastern flank of the anticyclonic anomaly in the tropical North Pacific, the end of the Rossby wave train, advects the low moist enthalpy air from the midlatitudes into the central tropical North Pacific and equatorial Pacific (dashed box in Fig. 8b). The negative moist enthalpy advection suppresses local convection (positive OLR anomalies) in the tropical North Pacific and equatorial central Pacific (dashed box in Fig. 5c), inducing a lower-level anomalous easterly from the equatorial central Pacific to Maritime Continent (from 180° to 120°E). The anomalous easterly could result in the negative SSTA in the equatorial central Pacific and further suppress the local convection in spring. The suppressed convection and negative SSTA strengthen and maintain the anomalous easterly through the Bjerknes positive

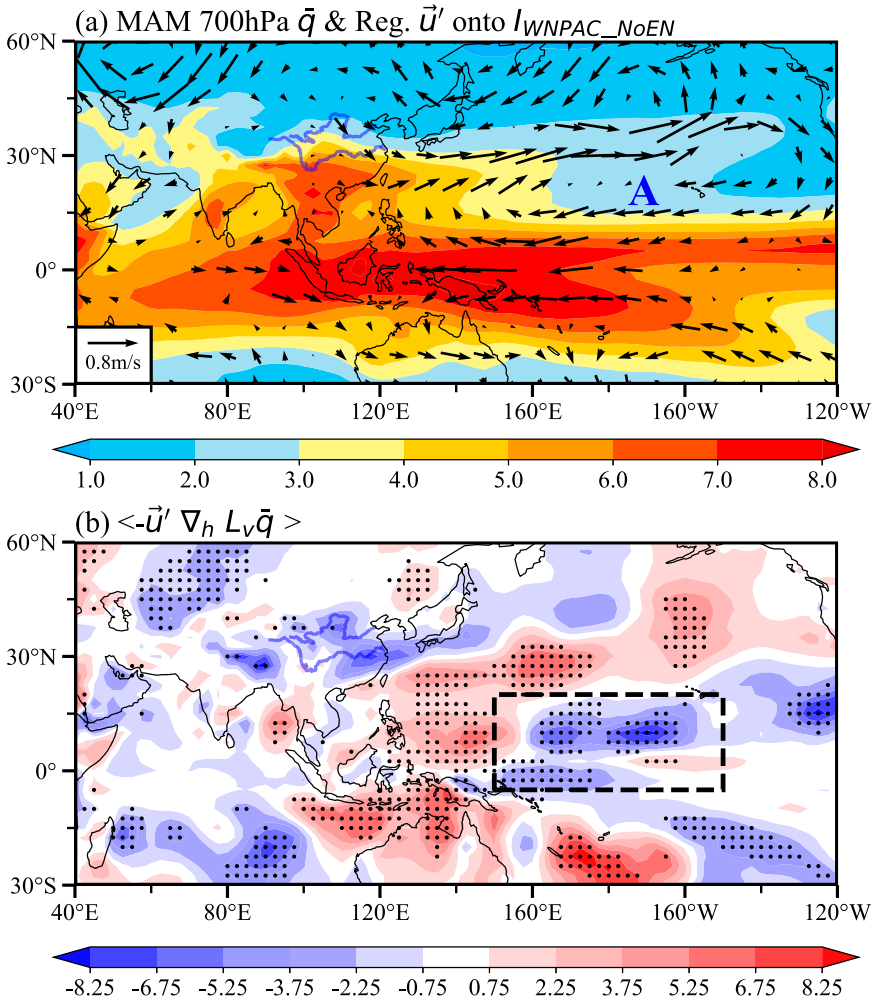

FIG. 8. (a) Regressed MAM 700-hPa climatological specific humidity (shading; g kg^{-1}) and anomalous winds (vectors; m s^{-1}) onto the JJA $I_{\mathrm{WNPAC\_NoEN}}$ index. (b) Regressed MAM horizontal advection of climatological specific humidity by the anomalous winds, which is converted to energy units (W m^{-2}). Stippled areas indicate the regression coefficients passing the 90% confidence level. The letter A in (a) denotes the center of anticyclonic anomaly. The black dashed box (5°S–20°N, 150°E–150°W) is as in Fig. 5c.

feedback, leading to a more remarkable zonal dipole anomalous SST and convection pattern over the Maritime Continent and equatorial western/central Pacific in summer (Figs. 5e,f). Because of the stronger anomalous easterly (from 120°W to 120°E) in summer, the anomalous zonal dipole convection in this season is stronger and shifted westward compared to that in spring. Consequently, the summer WNPAC is stimulated as a Gill-type response.

6. Summary and discussion

An MV-EOF analysis has been applied to the summer seasonal mean zonal and meridional wind over 0°–50°N, 100°–150°E to capture the main circulation feature over East Asia. The first EOF mode shows a dominant WNPAC, which accounts for 51% of the total variance. The WNPAC index (I_{WNPAC}) is highly consistent with the principal component (PC) of the first MV-EOF mode with a significant correlation coefficient of 0.95. Although the PC is significantly correlated with Niño-3.4 index, the ENSO–WNPAC relationship is unreliable.

Comparison of the two regressed SSTA patterns onto Niño-3.4 index and summer monthly WNPAC indices (I_{WNPAC}) show large differences over the tropical central/eastern Pacific and tropical Atlantic. To represent the influence of preceding ENSO in the following summer, the summer monthly I_{EN} indices have been defined as the tropical SSTA related to the previous winter Niño-3.4 index, which all have significant relationships with the corresponding I_{WNPAC} indices. After linearly removing the impacts of monthly I_{EN} indices, the WNPAC indices independent of ENSO ($I_{\mathrm{WNPAC\_NoEN}}$) differ from I_{WNPAC} indices only for some super El Niño events (Fig. 3). The almost unchanged WNPAC indices after the

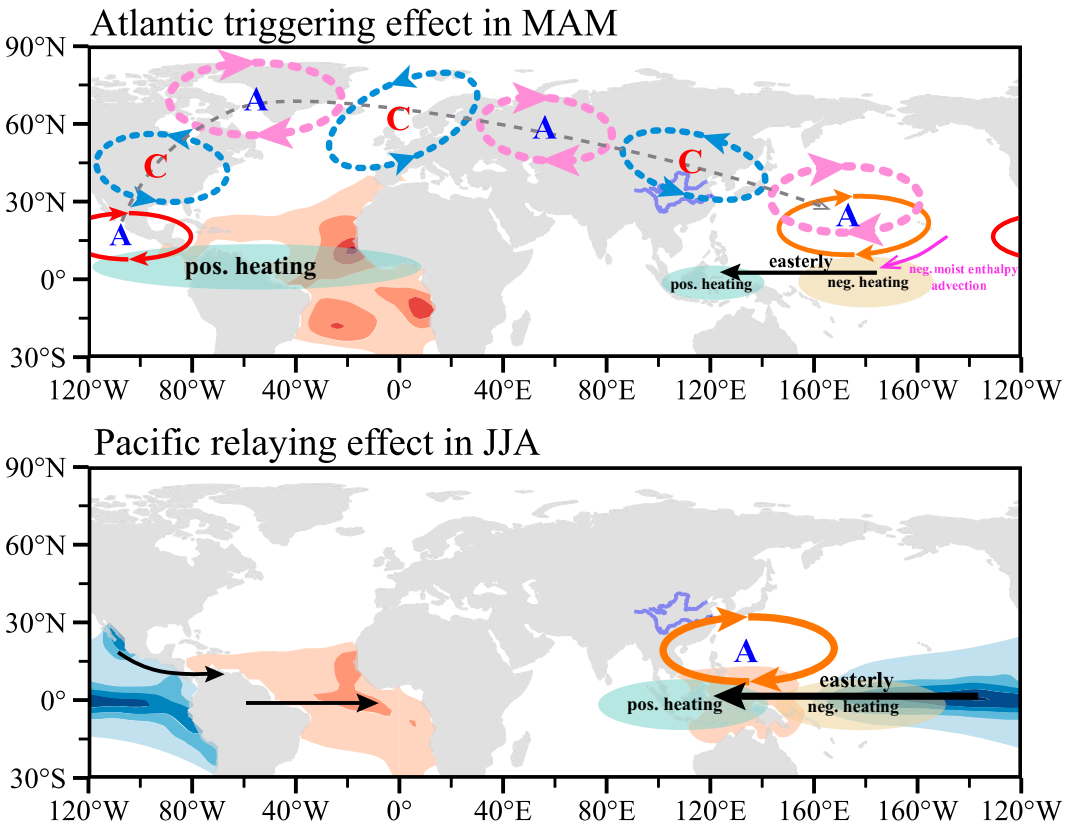

FIG. 9. Schematic diagram for the formation of WNPAC independent of ENSO. Red (blue) shadings denote the positive (negative) SSTA. Yellow (green) shadings indicate the negative (positive) diabatic heating anomalies. Letters C and A denote the cyclonic and anticyclonic anomalies, respectively. Blue cyclones and pink anticyclones with the gray dashed line represent the barotropic Rossby wave train. The red anticyclone in MAM denotes the tropical Rossby wave response at upper level. Orange anticyclones in MAM and JJA represent the lower-level anomalous anticyclone over the tropical North Pacific and the WNPAC, respectively. The pink arrow denotes the negative moist enthalpy advection, and the black ones denote the anomalous lower-level easterly (westerly/northwesterly) from the equatorial central Pacific to the Maritime Continent (from the eastern Pacific to the tropical Atlantic).

removal of ENSO's influence (except for the super El Niño years) indicate the limited contribution of ENSO on the summer WNPAC, suggesting the existence of other origins of the summer WNPAC.

The time evolutions of equatorial SSTA regressed onto I_{WNPAC} and $I_{\mathrm{WNPAC\_NoEN}}$ indices always show significant SSTA signals over the tropical Atlantic, indicating the fidelity of Atlantic oceanic forcing in the formation of WNPAC. In this study, an Atlantic-to-Pacific two-step mechanism for the formation of ENSO-independent WNPAC is proposed.

As shown in the schematic diagram (Fig. 9), the first step of the mechanism is the Atlantic triggering effect during springtime. In this stage, the positive Atlantic SSTAs could induce enhanced convection from equatorial eastern Pacific to Atlantic, which stimulates an upper-level anticyclonic anomaly over the Gulf of Mexico as a Gill-type response. This upper-level anomalous anticyclone acts as the Rossby wave source, leading to the equivalent barotropic Rossby wave train from North America to the Pacific following the great circle route, and thus causing a lower-level anomalous anticyclone over the tropical North Pacific. The anomalous northeasterly on the southeastern flank of the lower-level anomalous anticyclone advects low moist enthalpy air from the midlatitudes into the equatorial central Pacific, suppressing local convection and finally triggering the anomalous easterlies over the equatorial western/central Pacific. An anomalous zonal dipole convection pattern with enhanced (suppressed) convection in the Maritime Continent (central equatorial Pacific) then comes into being.

The second step of the mechanism is the Pacific relaying effect during summertime. The anomalous easterlies over the equatorial western/central Pacific in spring lead to negative SSTAs over the central tropical Pacific and positive SSTAs over the Maritime Continent. This dipole tropical SSTA pattern exerts a relaying effect, which further enhances the easterlies and leads to the intensified and westward shifted dipole convection anomalies, finally stimulating the summer WNPAC as a Gill-type response. Besides, the positive Atlantic SSTAs in summer can also induce lower-level northwesterly in tropical

eastern Pacific, which cools the eastern Pacific SST and further reinforces this coupled atmosphere–ocean interaction process.

The proposed Atlantic-to-Pacific two-step mechanism is validated in typical El Niño years such as 1988 and 1995, in which the WNPAC indices remained almost unchanged before and after removing ENSO's impacts (Fig. S6) despite the obvious El Niño events in previous winter (Niño-3.4 > 0.5). In spring, the Rossby wave train at the mid-to-high latitudes can be found in both years (Figs. S7a,b and S8a,b). The anomalous anticyclone over Gulf of Mexico, as the Gill-type response, stimulates the Rossby wave train and propagates to the tropical North Pacific. The anomalous northeasterly on the southeastern flank of the anomalous anticyclone advects negative moist enthalpy into the tropical Pacific, and contributes to the zonal dipole SSTA and convection in summer, inducing the WNPAC by Gill-type response (Figs. S7c,d and S8c,d).

However, it is not the case for the strong WNPAC in summer of 2020. In spring of 2020, an anomalous cyclone appears over tropical North Pacific, missing the key component of the Atlantic-to-Pacific two-step mechanism. Therefore, owing to its particularity, the strong WNPAC in summer 2020 cannot be traced back to the tropical Atlantic in previous spring. Although the positive SSTA over tropical western North Atlantic is considered to be one of the possible reasons for the strong WNPAC in summer 2020 (Wang et al. 2021), it seems that the crucial contributors of WNPAC in 2020 mainly include the Indian Ocean warming (Takaya et al. 2020; Pan et al. 2021; Tang et al. 2022; Zhou et al. 2021), Arctic sea ice loss (Chen et al. 2022; Li et al. 2022), and intraseasonal atmospheric signals such as the subseasonal phase transition of the NAO (Liu et al. 2020; Qiao et al. 2021) and the abnormal Madden–Julian oscillation (Zhang et al. 2021).

Previous studies have revealed that the negative SSTAs over the tropical central and eastern Pacific in summer induce and maintain the WNPAC via stimulating the Rossby wave response to the negative diabatic heating anomaly (Fan et al. 2013; Chen et al. 2016; Li et al. 2017; Jiang et al. 2019). However, these studies regard the negative SSTAs as a natural result of SSTA evolution from the previous El Niño episode to the La Niña episode. Here, we confirm that the negative SSTAs over the tropical central/eastern Pacific can enhance the summer WNPAC, but they are triggered by the atmospheric teleconnection induced by the positive Atlantic SSTAs through the extratropical route. We suggest that the Atlantic triggering effect in spring could also be one possible mechanism for the development of a La Niña event.

The Atlantic-to-Pacific two-step mechanism could provide a new reference for investigating the ENSO–WNPAC relationship. However, the relative contributions from ENSO-independent Atlantic SSTAs and ENSO-related SSTAs to the WNPAC merit further investigation, and seasonal prediction involving the predictability source from Atlantic should be carried out to further materialize our theoretical analysis.

Acknowledgments. This work was supported by the National Natural Science Foundation of China (Grants 42088101 and 42175033).

Data availability statement. The monthly sea surface temperature data from National Oceanic and Atmospheric Administration (NOAA) Extended Reconstructed SST version 5 are available at https://psl.noaa.gov/data/gridded/data.noaa.ersst.v5.html. The interpolated monthly outgoing longwave radiation data are provided by NOAA at https://psl.noaa.gov/data/gridded/data.interp_OLR.html. The monthly precipitation data are obtained by Global Precipitation Climatology Project at https://psl.noaa.gov/data/gridded/data.gpcp.html. The monthly wind and geopotential height data from the National Center for Environmental Prediction–National Center for Atmospheric Research Reanalysis are available at https://psl.noaa.gov/data/gridded/data.ncep.reanalysis.html. The monthly wind, geopotential height and specific humidity data from the fifth-generation ECMWF reanalysis for the global climate and weather are openly obtained at https://cds.climate.copernicus.eu/cdsapp#!/search?type=dataset&text=ERA5.

REFERENCES

Adler, R. F., and Coauthors, 2003: The version 2 Global Precipitation Climatology Project (GPCP) monthly precipitation analysis (1979–present). *J. Hydrometeor.*, **4**, 1147–1167, https://doi.org/10.1175/1525-7541(2003)004<1147:TVGPCP>2.0.CO;2.

Chang, C.-P., Y. Zhang, and T. Li, 2000: Interannual and interdecadal variations of the East Asian summer monsoon and tropical Pacific SSTs. Part I: Roles of the subtropical ridge. *J. Climate*, **13**, 4310–4325, https://doi.org/10.1175/1520-0442(2000)013<4310:IAIVOT>2.0.CO;2.

Chen, S., W. Chen, B. Yu, and Z. Li, 2022: Impact of internal climate variability on the relationship between spring northern tropical Atlantic SST anomalies and succedent winter ENSO: The role of the North Pacific Oscillation. *J. Climate*, **35**, 537–559, https://doi.org/10.1175/JCLI-D-21-0505.1.

Chen, X., A. Dai, Z. Wen, and Y. Song, 2021: Contributions of Arctic sea-ice loss and East Siberian atmospheric blocking to 2020 record-breaking Meiyu-Baiu rainfall. *Geophys. Res. Lett.*, **48**, e2021GL092748, https://doi.org/10.1029/2021GL092748.

Chen, Z., Z. Wen, R. Wu, X. Lin, and J. Wang, 2016: Relative importance of tropical SST anomalies in maintaining the western North Pacific anomalous anticyclone during El Niño to La Niña transition years. *Climate Dyn.*, **46**, 1027–1041, https://doi.org/10.1007/s00382-015-2630-1.

Chou, C., 2004: Establishment of the low-level wind anomalies over the western North Pacific during ENSO development. *J. Climate*, **17**, 2195–2212, https://doi.org/10.1175/1520-0442(2004)017<2195:EOTLWA>2.0.CO;2.

——, L.-F. Huang, J.-Y. Tu, L. Tseng, and Y.-C. Hsueh, 2009: El Niño impacts on precipitation in the western North Pacific–East Asian sector. *J. Climate*, **22**, 2039–2057, https://doi.org/10.1175/2008JCLI2649.1.

Enomoto, T., 2004: Interannual variability of the Bonin high associated with the propagation of Rossby waves along the Asian jet. *J. Meteor. Soc. Japan*, **82**, 1019–1034, https://doi.org/10.2151/jmsj.2004.1019.

Exarchou, E., P. Ortega, B. Rodríguez-Fonseca, T. Losada, I. Polo, and C. Prodhomme, 2021: Impact of equatorial Atlantic variability on ENSO predictive skill. *Nat. Commun.*, **12**, 1612, https://doi.org/10.1038/s41467-021-21857-2.

Fan, L., S.-I. Shin, Q. Liu, and Z. Liu, 2013: Relative importance of tropical SST anomalies in forcing East Asian summer

monsoon circulation. *Geophys. Res. Lett.*, **40**, 2471–2477, https://doi.org/10.1002/grl.50494.

Gao, M., J. Yang, D. Gong, and S.-J. Kim, 2014: Unstable relationship between spring Arctic Oscillation and East Asian summer monsoon. *Int. J. Climatol.*, **34**, 2522–2528, https://doi.org/10.1002/joc.3849.

——, ——, ——, H. He, and S.-J. Kim, 2016: Spring Arctic Oscillation–western North Pacific connection in CMIP5 models. *Int. J. Climatol.*, **36** (4), 2093–2102, https://doi.org/10.1002/joc.4486.

Gill, A. E., 1980: Some simple solutions for heat-induced tropical circulation. *Quart. J. Roy. Meteor. Soc.*, **106**, 447–462, https://doi.org/10.1002/qj.49710644905.

Gong, D.-Y., J. Yang, S.-J. Kim, Y. Gao, D. Guo, T. Zhou, and M. Hu, 2011: Spring Arctic Oscillation–East Asian summer monsoon connection through circulation changes over the western North Pacific. *Climate Dyn.*, **37**, 2199–2216, https://doi.org/10.1007/s00382-011-1041-1.

Ham, Y.-G., J.-S. Kug, J.-Y. Park, and F.-F. Jin, 2013: Sea surface temperature in the north tropical Atlantic as a trigger for El Niño/Southern Oscillation events. *Nat. Geosci.*, **6**, 112–116, https://doi.org/10.1038/ngeo1686.

Held, I. M., and M. J. Suarez, 1994: A proposal for the intercomparison of the dynamical cores of atmospheric general circulation models. *Bull. Amer. Meteor. Soc.*, **75**, 1825–1830, https://doi.org/10.1175/1520-0477(1994)075<1825:APFTIO>2.0.CO;2.

Hersbach, H., and Coauthors, 2019: ERA5 monthly averaged data on pressure levels from 1979 to present. C3S CDS, accessed 4 August 2021, https://doi.org/10.24381/cds.6860a573.

Hong, C.-C., T.-C. Chang, and H.-H. Hsu, 2014: Enhanced relationship between the tropical Atlantic SST and the summertime western North Pacific subtropical high after the early 1980s. *J. Geophys. Res. Atmos.*, **119**, 3715–3722, https://doi.org/10.1002/2013JD021394.

Hoskins, B. J., and D. J. Karoly, 1981: The steady linear response of a spherical atmosphere to thermal and orographic forcing. *J. Atmos. Sci.*, **38**, 1179–1196, https://doi.org/10.1175/1520-0469(1981)038<1179:TSLROA>2.0.CO;2.

Huang, B., and Coauthors, 2017: Extended Reconstructed Sea Surface Temperature, version 5 (ERSSTv5): Upgrades, validations, and intercomparisons. *J. Climate*, **30**, 8179–8205, https://doi.org/10.1175/JCLI-D-16-0836.1.

Huang, R., and Y. Wu, 1989: The influence of ENSO on the summer climate change in China and its mechanism. *Adv. Atmos. Sci.*, **6**, 21–32, https://doi.org/10.1007/BF02656915.

Jiang, L., and T. Li, 2021: Impacts of tropical North Atlantic and equatorial Atlantic SST anomalies on ENSO. *J. Climate*, **34**, 5635–5655, https://doi.org/10.1175/JCLI-D-20-0835.1.

Jiang, W., G. Huang, P. Huang, R. Wu, K. Hu, and W. Chen, 2019: Northwest Pacific anticyclonic anomalies during post–El Niño summers determined by the pace of El Niño decay. *J. Climate*, **32**, 3487–3503, https://doi.org/10.1175/JCLI-D-18-0793.1.

Kalnay, E., and Coauthors, 1996: The NCEP/NCAR 40-Year Reanalysis Project. *Bull. Amer. Meteor. Soc.*, **77**, 437–472, https://doi.org/10.1175/1520-0477(1996)077<0437:TNYRP>2.0.CO;2.

Kosaka, Y., J. S. Chowdary, S.-P. Xie, Y.-M. Min, and J.-Y. Lee, 2012: Limitations of seasonal predictability for summer climate over East Asia and the northwestern Pacific. *J. Climate*, **25**, 7574–7589, https://doi.org/10.1175/JCLI-D-12-00009.1.

Li, H., B. Sun, H. Wang, and X. Yuan, 2022: Joint effects of three oceans on the 2020 super mei-yu. *Atmos. Oceanic Sci. Lett.*, **15**, 100127, https://doi.org/10.1016/j.aosl.2021.100127.

Li, T., B. Wang, B. Wu, T. Zhou, C.-P. Chang, and R. Zhang, 2017: Theories on formation of an anomalous anticyclone in western North Pacific during El Niño: A review. *J. Meteor. Res.*, **31**, 987–1006, https://doi.org/10.1007/s13351-017-7147-6.

Liebmann, B., and C. A. Smith, 1996: Description of a complete (interpolated) outgoing longwave radiation dataset. *Bull. Amer. Meteor. Soc.*, **77**, 1275–1277, https://doi.org/10.1175/1520-0477-77.6.1274.

Liu, B., Y. Yan, C. Zhu, S. Ma, and J. Li, 2020: Record-breaking Meiyu rainfall around the Yangtze River in 2020 regulated by the subseasonal phase transition of the North Atlantic Oscillation. *Geophys. Res. Lett.*, **47**, e2020GL090342, https://doi.org/10.1029/2020GL090342.

Lu, R., Z. Zhu, T. Li, and H. Zhang, 2020: Interannual and interdecadal variabilities of spring rainfall over Northeast China and their associated sea surface temperature anomaly forcings. *J. Climate*, **33**, 1423–1435, https://doi.org/10.1175/JCLI-D-19-0302.1.

Neelin, J. D., 2007: Moist dynamics of tropical convection zones in monsoons, teleconnections, and global warming. *The Global Circulation of the Atmosphere*, T. Schneider and A. Sobel, Eds., Princeton University Press, 267–301.

——, and I. M. Held, 1987: Modeling tropical convergence based on the moist static energy budget. *Mon. Wea. Rev.*, **115**, 3–12, https://doi.org/10.1175/1520-0493(1987)115<0003:MTCBOT>2.0.CO;2.

North, G. R., T. L. Bell, R. F. Cahalan, and F. J. Moeng, 1982: Sampling errors in the estimation of empirical orthogonal functions. *Mon. Wea. Rev.*, **110**, 699–706, https://doi.org/10.1175/1520-0493(1982)110<0699:SEITEO>2.0.CO;2.

Pan, X., T. Li, Y. Sun, and Z. Zhu, 2021: Cause of extreme heavy and persistent rainfall over Yangtze River in summer 2020. *Adv. Atmos. Sci.*, **38**, 1994–2009, https://doi.org/10.1007/s00376-021-0433-3.

Park, J.-H., J.-S. Kug, Y.-M. Yang, H. Oh, J. Zhao, and Y. Wu, 2022: Role of climatological North Pacific high in the north tropical Atlantic–ENSO connection. *J. Climate*, **35**, 3215–3226, https://doi.org/10.1175/JCLI-D-21-0933.1.

Qiao, S., and Coauthors, 2021: The longest 2020 Meiyu season over the past 60 years: Subseasonal perspective and its predictions. *Geophys. Res. Lett.*, **48**, e2021GL093596, https://doi.org/10.1029/2021GL093596.

Rong, X., R. Zhang, and T. Li, 2010: Impacts of Atlantic sea surface temperature anomalies on Indo-East Asian summer monsoon–ENSO relationship. *Chin. Sci. Bull.*, **55**, 2458–2468, https://doi.org/10.1007/s11434-010-3098-3.

Sampe, T., and S.-P. Xie, 2010: Large-scale dynamics of the meiyu-baiu rainband: Environmental forcing by the westerly jet. *J. Climate*, **23**, 113–134, https://doi.org/10.1175/2009JCLI3128.1.

Takaya, K., and H. Nakamura, 2001: A formulation of a phase-independent wave-activity flux for stationary and migratory quasigeostrophic eddies on a zonally varying basic flow. *J. Atmos. Sci.*, **58**, 608–627, https://doi.org/10.1175/1520-0469(2001)058<0608:AFOAPI>2.0.CO;2.

Takaya, Y., I. Ishikawa, C. Kobayashi, H. Endo, and T. Ose, 2020: Enhanced Meiyu-Baiu rainfall in early summer 2020: Aftermath of the 2019 super IOD event. *Geophys. Res. Lett.*, **47**, e2020GL090671, https://doi.org/10.1029/2020GL090671.

Tang, S., S. Qiao, T. Feng, Z. Fu, Z. Zhang, and G. Feng, 2022: Predictability of the record-breaking rainfall over the Yangtze and Huaihe River valley in 2020 summer by the NCEP CFSv2. *Atmos. Res.*, **266**, 105956, https://doi.org/10.1016/j.atmosres.2021.105956.

Wang, B., 1992: The vertical structure and development of the ENSO anomaly mode during 1979–1989. *J. Atmos. Sci.*, **49**, 698–712, https://doi.org/10.1175/1520-0469(1992)049<0698:TVSADO>2.0.CO;2.

——, and J. C. L. Chan, 2002: How strong ENSO events affect tropical storm activity over the western North Pacific. *J. Climate*, **15**, 1643–1658, https://doi.org/10.1175/1520-0442(2002)015<1643:HSEEAT>2.0.CO;2.

——, and Q. Zhang, 2002: Pacific–East Asian teleconnection. Part II: How the Philippine Sea anomalous anticyclone is established during El Niño development. *J. Climate*, **15**, 3252–3265, https://doi.org/10.1175/1520-0442(2002)015<3252:PEATPI>2.0.CO;2.

——, R. Wu, and X. Fu, 2000: Pacific–East Asian teleconnection: How does ENSO affect East Asian climate? *J. Climate*, **13**, 1517–1536, https://doi.org/10.1175/1520-0442(2000)013<1517:PEATHD>2.0.CO;2.

——, Z. Wu, J. Li, J. Liu, C.-P. Chang, Y. Ding, and G. Wu, 2008: How to measure the strength of the East Asian summer monsoon. *J. Climate*, **21**, 4449–4463, https://doi.org/10.1175/2008JCLI2183.1.

——, B. Xiang, and J.-Y. Lee, 2013: Subtropical high predictability establishes a promising way for monsoon and tropical storm predictions. *Proc. Natl. Acad. Sci. USA*, **110**, 2718–2722, https://doi.org/10.1073/pnas.1214626110.

——, J. Li, and Q. He, 2017: Variable and robust East Asian monsoon rainfall response to El Niño over the past 60 years (1957–2016). *Adv. Atmos. Sci.*, **34**, 1235–1248, https://doi.org/10.1007/s00376-017-7016-3.

Wang, C., and B. Wang, 2019: Tropical cyclone predictability shaped by western Pacific subtropical high: Integration of trans-basin sea surface temperature effects. *Climate Dyn.*, **53**, 2697–2714, https://doi.org/10.1007/s00382-019-04651-1.

Wang, C.-Y., S.-P. Xie, and K. Yu, 2018: Indo-western Pacific climate variability: ENSO forcing and internal dynamics in a tropical Pacific pacemaker simulation. *J. Climate*, **31**, 10 123–10 139, https://doi.org/10.1175/JCLI-D-18-0203.1.

——, ——, and ——, 2020: ENSO-unrelated variability in Indo-northwest Pacific climate: Regional coupled ocean–atmospheric feedback. *J. Climate*, **33**, 4095–4108, https://doi.org/10.1175/JCLI-D-19-0426.1.

Wang, C. Z., Y. Yao, H. Wang, X. Sun, and J. Zheng, 2021: The 2020 summer floods and 2020/21 winter extreme cold surges in China and the 2020 typhoon season in the western North Pacific. *Adv. Atmos. Sci.*, **38**, 896–904, https://doi.org/10.1007/s00376-021-1094-y.

Wang, W., W. Zhou, and D. Chen, 2014: Summer high temperature extremes in Southeast China: Bonding with the El Niño–Southern Oscillation and East Asian summer monsoon coupled system. *J. Climate*, **27**, 4122–4138, https://doi.org/10.1175/JCLI-D-13-00545.1.

Wang, Y., B. Wu, and T. Zhou, 2022: Maintenance of western North Pacific anomalous anticyclone in boreal summer by wind-induced moist enthalpy advection mechanism. *J. Climate*, **35**, 4499–4511, https://doi.org/10.1175/JCLI-D-21-0708.1.

Watanabe, M., and M. Kimoto, 2000: Atmosphere–ocean thermal coupling in the North Atlantic: A positive feedback. *Quart. J. Roy. Meteor. Soc.*, **126**, 3343–3369, https://doi.org/10.1002/qj.49712657017; Corrigendum, **127**, 733–734, https://doi.org/10.1002/qj.49712757223.

Wu, B., T. Zhou, and T. Li, 2009: Contrast of rainfall–SST relationships in the western North Pacific between the ENSO-developing and ENSO-decaying summers. *J. Climate*, **22**, 4398–4405, https://doi.org/10.1175/2009JCLI2648.1.

——, T. Li, and T. Zhou, 2010: Relative contributions of the Indian Ocean and local SST anomalies to the maintenance of the western North Pacific anomalous anticyclone during the El Niño decaying summer. *J. Climate*, **23**, 2974–2986, https://doi.org/10.1175/2010JCLI3300.1.

——, T. Zhou, and T. Li, 2017a: Atmospheric dynamic and thermodynamic processes driving the western North Pacific anomalous anticyclone during El Niño. Part I: Maintenance mechanisms. *J. Climate*, **30**, 9621–9635, https://doi.org/10.1175/JCLI-D-16-0489.1.

——, ——, and ——, 2017b: Atmospheric dynamic and thermodynamic processes driving the western North Pacific anomalous anticyclone during El Niño. Part II: Formation processes. *J. Climate*, **30**, 9637–9650, https://doi.org/10.1175/JCLI-D-16-0495.1.

Wu, R., Z.-Z. Hu, and B. P. Kirtman, 2003: Evolution of ENSO-related rainfall anomalies in East Asia. *J. Climate*, **16**, 3742–3758, https://doi.org/10.1175/1520-0442(2003)016<3742:EOERAI>2.0.CO;2.

Wu, Z., B. Wang, J. Li, and F.-F. Jin, 2009: An empirical seasonal prediction model of the East Asian summer monsoon using ENSO and NAO. *J. Geophys. Res.*, **114**, D18120, https://doi.org/10.1029/2009JD011733.

——, J. Li, Z. Jiang, J. He, and X. Zhu, 2012: Possible effects of the North Atlantic Oscillation on the strengthening relationship between the East Asian summer monsoon and ENSO. *Int. J. Climatol.*, **32**, 794–800, https://doi.org/10.1002/joc.2309.

Xie, S.-P., K. Hu, J. Hafner, H. Tokinaga, Y. Du, G. Huang, and T. Sampe, 2009: Indian Ocean capacitor effect on Indo-western Pacific climate during the summer following El Niño. *J. Climate*, **22**, 730–747, https://doi.org/10.1175/2008JCLI2544.1.

Yang, J., Q. Liu, and Z. Liu, 2010: Linking observations of the Asian monsoon to the Indian Ocean SST: Possible roles of Indian Ocean basin mode and dipole mode. *J. Climate*, **23**, 5889–5902, https://doi.org/10.1175/2010JCLI2962.1.

Yang, Y., Z. Zhu, X. Shen, L. Jiang, and T. Li, 2023: The influences of Atlantic sea surface temperature anomalies on the ENSO-independent interannual variability of East Asian summer monsoon rainfall. *J. Climate*, **36**, 677–692, https://doi.org/10.1175/JCLI-D-22-0061.1.

Yu, J., T. Li, Z. Tan, and Z. Zhu, 2016: Effects of tropical North Atlantic SST on tropical cyclone genesis in the western North Pacific. *Climate Dyn.*, **46**, 865–877, https://doi.org/10.1007/s00382-015-2618-x.

Zhang, P., Y. Liu, and B. He, 2016: Impact of East Asian summer monsoon heating on the interannual variation of the South Asian high. *J. Climate*, **29**, 159–173, https://doi.org/10.1175/JCLI-D-15-0118.1.

Zhang, R., A. Sumi, and M. Kimoto, 1996: Impact of El Niño on the East Asian monsoon: A diagnostic study of the '86/87 and '91/92 events. *J. Meteor. Soc. Japan*, **74**, 49–62, https://doi.org/10.2151/jmsj1965.74.1_49.

——, ——, and ——, 1999: A diagnostic study of the impact of El Niño on the precipitation in China. *Adv. Atmos. Sci.*, **16**, 229–241, https://doi.org/10.1007/BF02973084.

Zhang, W., Z. Huang, F. Jiang, M. Stuecker, G. Chen, and F.-F. Jin, 2021: Exceptionally persistent Madden–Julian Oscillation

activity contributes to the extreme 2020 East Asian summer monsoon rainfall. *Geophys. Res. Lett.*, **48**, e2020GL091588, https://doi.org/10.1029/2020GL091588.

Zhao, Y., J. Cheng, G. Feng, Z. Zheng, R. Zhi, Z. Zhang, J. Yan, and D. Zuo, 2022: Dominant role of meridional circulation in regulating the anomalous subsidence of the western Pacific subtropical high in early summer 2020. *Front. Phys.*, **10**, 713087, https://doi.org/10.3389/fphy.2022.713087.

Zheng, J., and C. Wang, 2021: Influences of three oceans on record-breaking rainfall over the Yangtze River Valley in June 2020. *Sci. China Earth Sci.*, **64**, 1607–1618, https://doi.org/10.1007/s11430-020-9758-9.

Zhou, Z.-Q., S.-P. Xie, and R. Zhang, 2021: Historic Yangtze flooding of 2020 tied to extreme Indian Ocean conditions. *Proc. Natl. Acad. Sci. USA*, **118**, e2022255118, https://doi.org/10.1073/pnas.2022255118.

Zhu, Z., and T. Li, 2016: A new paradigm for the continental United States summer rainfall variability: Asia–North America teleconnection. *J. Climate*, **29**, 7313–7327, https://doi.org/10.1175/JCLI-D-16-0137.1.

——, and ——, 2018: Amplified contiguous United States summer rainfall variability induced by East Asian monsoon interdecadal change. *Climate Dyn.*, **50**, 3523–3536, https://doi.org/10.1007/s00382-017-3821-8.

Zuo, J., W. Li, C. Sun, and H.-C. Ren, 2019: Remote forcing of the northern tropical Atlantic SST anomalies on the western North Pacific anomalous anticyclone. *Climate Dyn.*, **52**, 2837–2853, https://doi.org/10.1007/s00382-018-4298-9.

Supplemental Material

Supplementary information for:

Formation mechanism of the ENSO-independent summer western North Pacific anomalous anticyclone

Tong Lu[1, 2, 3], Zhiwei Zhu[1, 2*], Ying Yang[1], Jing Ma[1], Gang Huang[2, 3]

1, Key Laboratory of Meteorological Disaster, Ministry of Education (KLME)/Joint International Research Laboratory of Climate and Environment Change (ILCEC)/Collaborative Innovation Center on Forecast and Evaluation of Meteorological Disasters (CIC-FEMD), Nanjing University of Information Science and Technology, Nanjing, China
2, State Key Laboratory of Numerical Modeling for Atmospheric Sciences and Geophysical Fluid Dynamics, Institute of Atmospheric Physics, Chinese Academy of Sciences, Beijing, China
3, University of Chinese Academy of Sciences, Beijing 100049, China

This file includes:

Supplementary Table S1 and Figures S1-S8.

Corresponding author: Zhiwei Zhu, Nanjing University of Information Science and Technology, Ningliu Road 219, Meteorology Bldg. Jiangsu 210044, China. E-mail: zwz@nuist.edu.cn

Table S1. The El Niño years with the absolute values of the differences between monthly I_{WNPAC} and I_{WNPAC_NoEN} exceeding the corresponding thresholds in June, July and August. The thresholds are defined by arranging the absolute values of all the differences in descending order and taking the 5th percentile. The bold words denote strong events.

June (0.56)	**1983**	**1998**
July (1.21)	1987	**1998**
August (0.89)	**1998**	**2016**

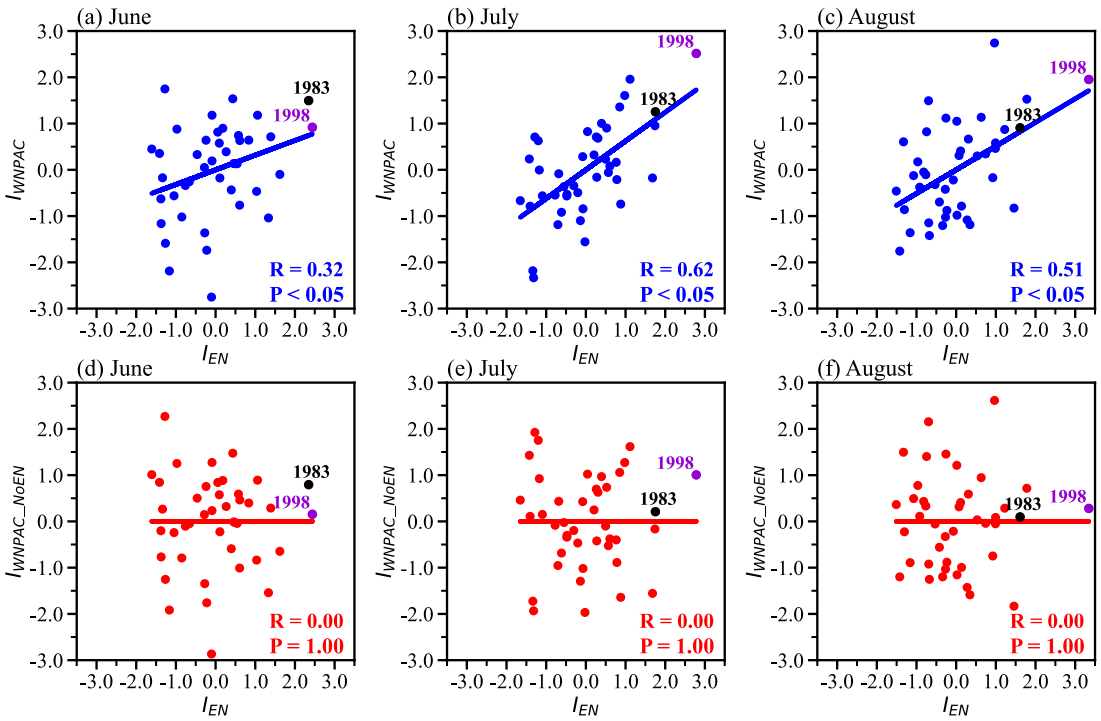

Fig. S1. Scatter plots between (a) the I_{EN} and I_{WNPAC} index (blue dots), and (d) the I_{EN} and I_{WNPAC_NoEN} index (red dots) in June; (b, e) and (c, f) same as (a, d), but for that in July and August. Black and purple dots indicate the results in 1983 and 1998, respectively.

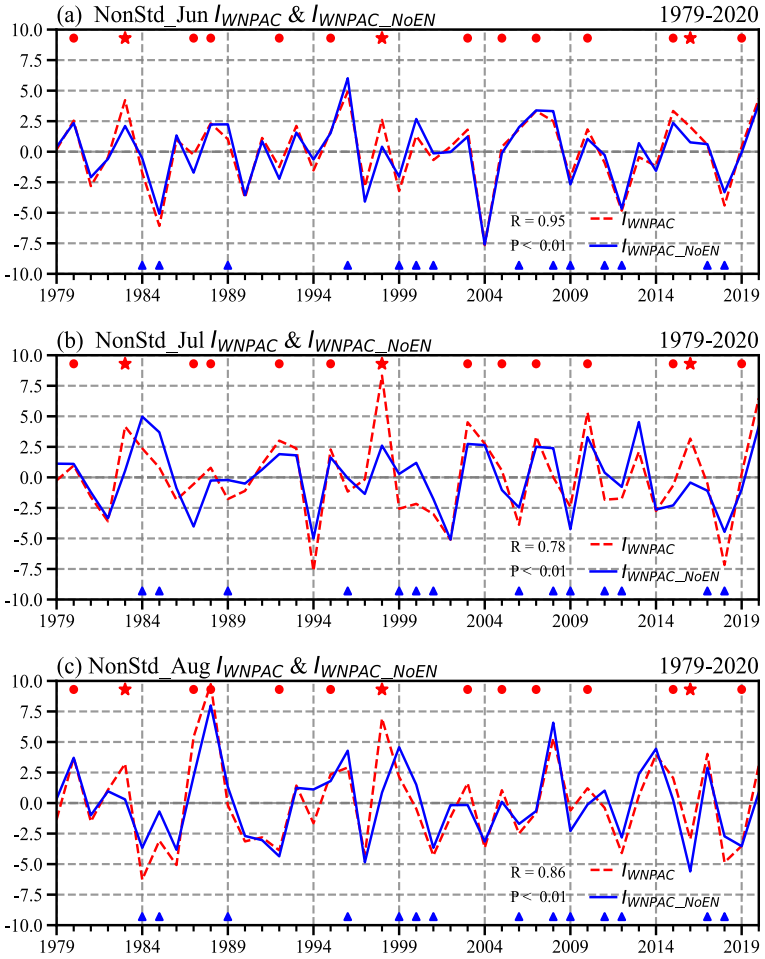

Fig. S2. Same as Fig. 3, but for the indices without being standardized.

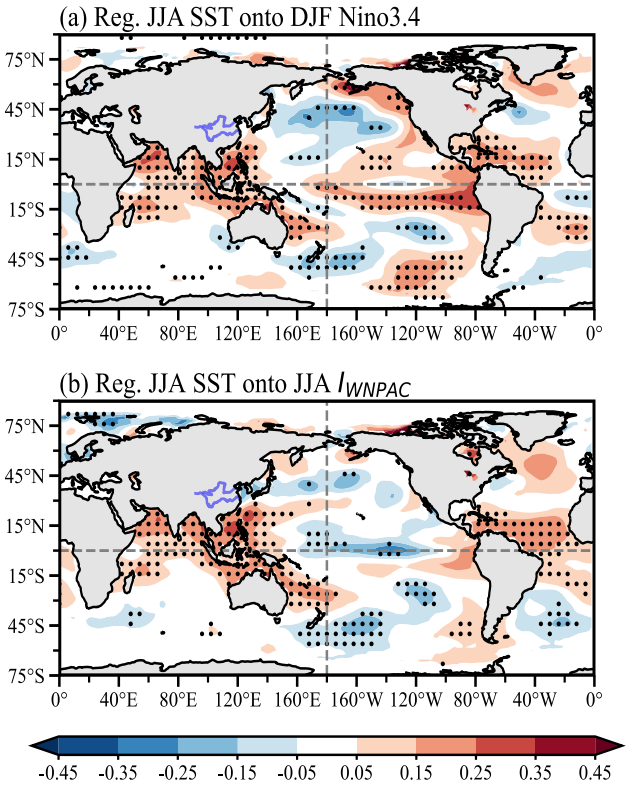

Fig. S3. The JJA global SST (shading, °C) regressed onto the (a) DJF Niño3.4 and (b) JJA I_{WNPAC} indices. Stippling areas indicate regression coefficients passing the 95% confidence level. The vertical and horizontal dashed lines denote the 180° meridian and the equator, respectively.

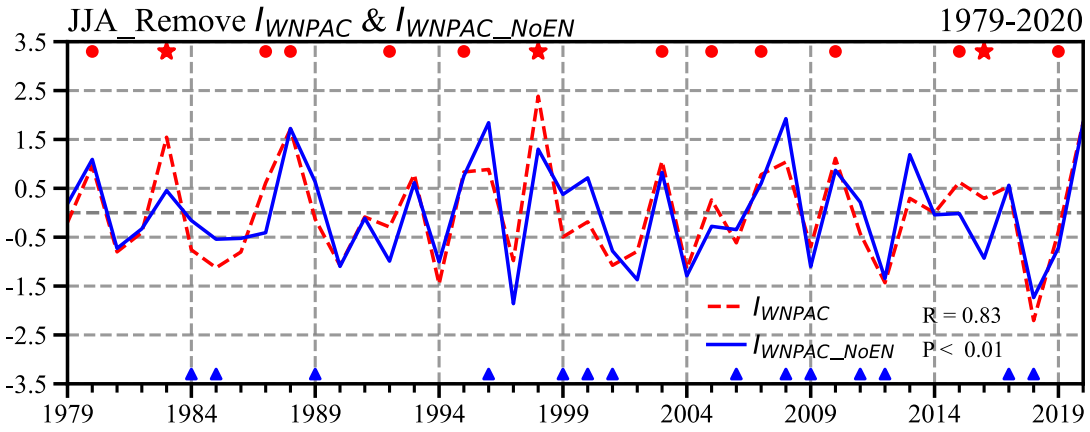

Fig. S4. The WNPAC index (I_{WNPAC}, red dashed lines) and the WNPAC index after removing ENSO's impact (I_{WNPAC_NoEN}, blue solid lines) in JJA directly. The red dots and blue triangles denote the El Niño and La Niña years, respectively. The red stars represent the three super El Niño years of 1983, 1998 and 2016.

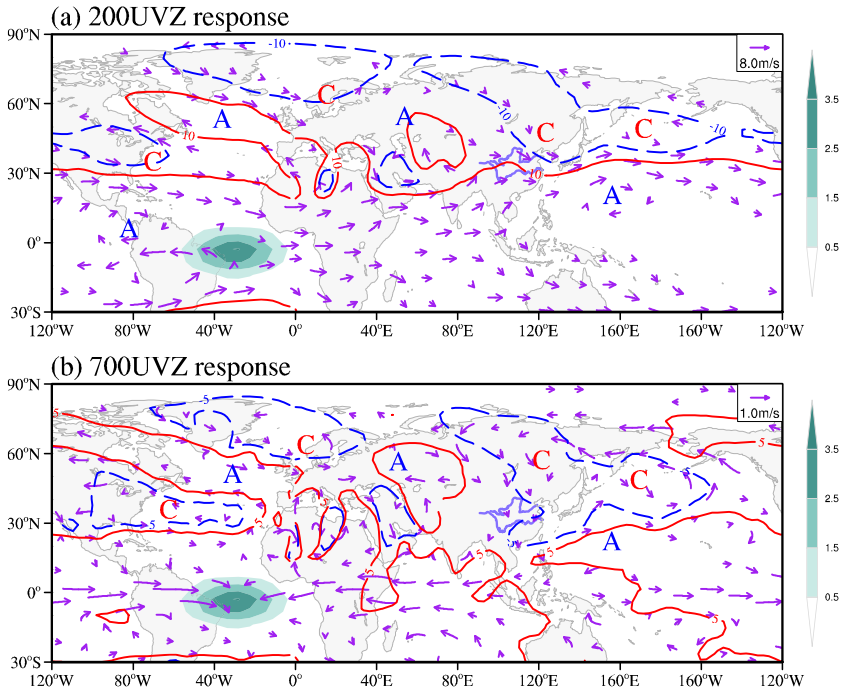

Fig. S5. The (a) 200-hPa and (b) 700-hPa wind (vectors; m s^{-1}) and geopotential height (contours; gpm) response to idealized heating centered at 4° S, 30° W in LBM experiment. The letters A and C denote the centers of the anticyclonic and cyclonic anomalies, respectively.

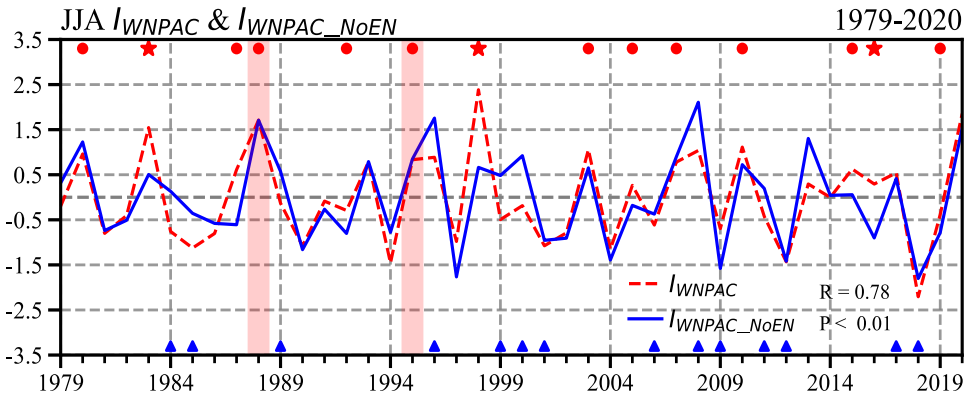

Fig. S6. The comparison between summer mean WNPAC index before (I_{WNPAC}, red dashed lines) and after (I_{WNPAC_NoEN}, blue solid lines) removing monthly ENSO's impact. The red dots and blue triangles denote the El Niño and La Niña years respectively and the red stars represent the three super El Niño years of 1983, 1998 and 2016. The red bars indicate the El Niño years with smaller differences between I_{WNPAC} and I_{WNPAC_NoEN}, which can validate the Atlantic-to-Pacific two-step mechanism.

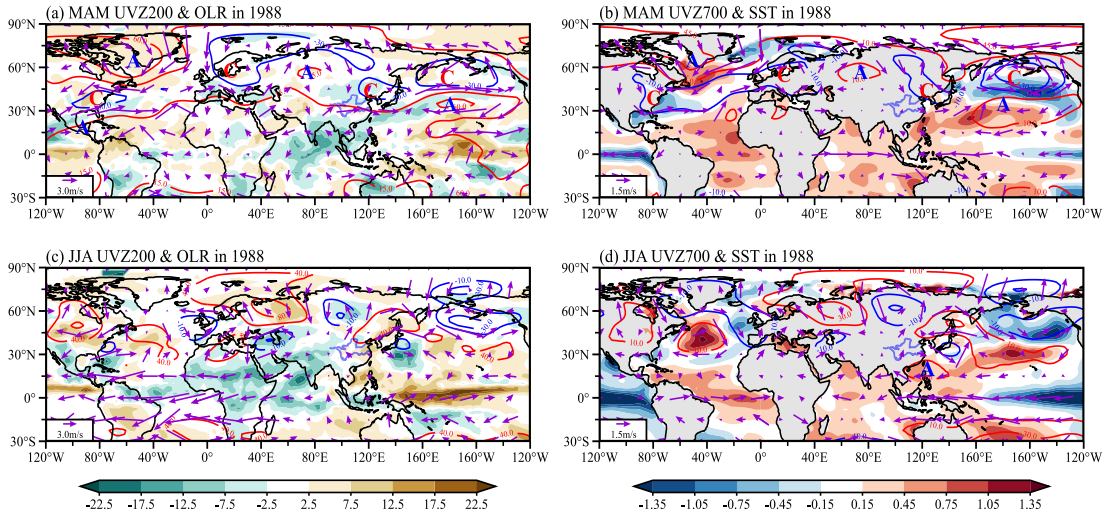

Fig. S7. The anomalous (a) 200-hPa wind (vectors; m s^{-1}), geopotential height (contours; gpm) and OLR (shadings; W m^{-2}), and (b) 700-hPa wind (vectors; m s^{-1}), geopotential height (contours; gpm) and SST (shadings; °C) in MAM 1988. (c–d) is the same as (a–b) but for that in JJA, respectively. The letter A/C denotes the center of the anticyclonic/cyclonic anomalies.

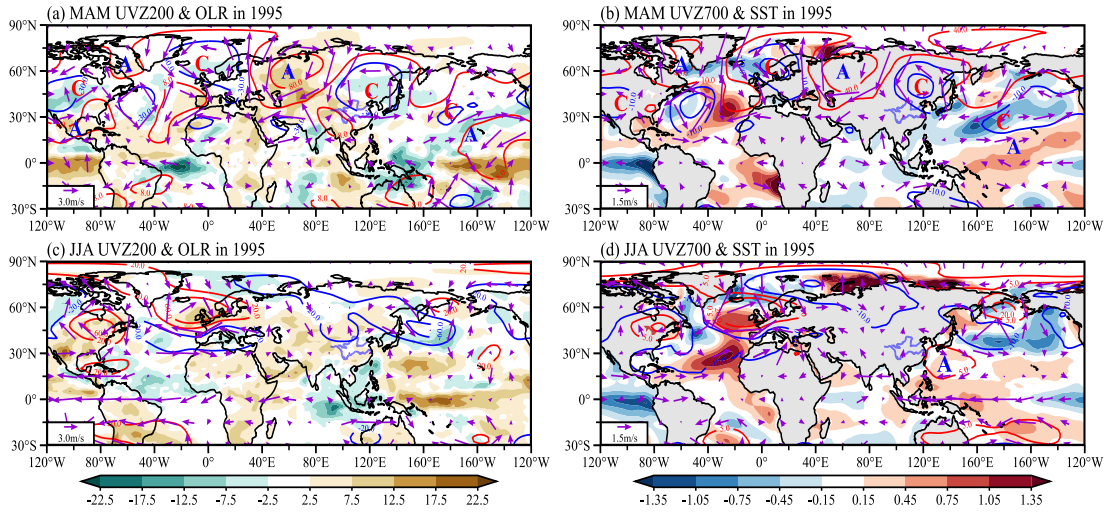

Fig. S8. Same as Fig. S7, but for 1995.